NDOT Research Report

Report No: RDT95-012

NONLINEAR BRIDGE ABUTMENT STIFFNESSES: FORMULATION VERIFICATION and DESIGN CURVES

July 2001

Prepared by Research Division
Nevada Department of Transportation
1263 South Stewart Street
Carson City, Nevada 89712

NEVADA DOT

TECHNICAL REPORT DOCUMENTATION PAGE

Report No. **RDT 95-012**	2. Government Accession No.	3. Recipient's Catalog No.

4. Title and Subtitle **Nonlinear Bridge Abutment Stiffnesses: Formulation Verification and Design Curves**	5. Report Date **June 1995**
	6. Performing Organization Code
7. Author(s) **Raj Siddhartan, Mahmoud El-Gamal, Emmanuel A. Margakis**	8. Performing Organization Report No.
9. Performing Organization Name and Address **Nevada Department of Transportation** **1263 S. Stewart Street** **Carson City, NV 89712**	10. Work Unit No.
	11. Contract or Grant No. P009-93/028
12. Sponsoring Agency Name and Address **Nevada Department of Transportation** **1263 South Stewart** **Carson City, Nevada 89712**	13. Type or Report and Period Covered January 1993 - To June 1995
	14. Sponsoring Agency Code **NDOT**

15. Supplementary Notes

16. Abstract

This report presents an efficient approach to evaluate the nonlinear translational spring stiffnesses to represent seat-type abutments. The applicability of previous studies is limited because such studies are incapable of handling many important factors such as the nonlinear soil behavior, the free-field strains induced by an earthquake, the influence of wing walls, and the difference in soil behavior under active and passive conditions. The proposed approach accounts for all of these factors. The procedures adopted in this approach are relatively simple, and emphasis has been placed on easy interpretation and on achieving consistency between design procedures routinely used in the static and seismic design of abutments. Only routinely used soil properties, such as the relative density, unit weight, angle of internal friction, and interface friction angles, are required.

The proposed approach has been used to develop ready to use design curves to estimate abutment stiffnesses. The design curves have been developed as a function of the height and width of the abutment and the seismic coefficient, k_h (Equation 16). Modification factors have also been developed to account for changes in the baseline parameters used in the development of the design curves (Equation 19). The applicability of the proposed approach has also been verified using recently completed large-scale abutment field tests.

17. Key Words	18. Distribution Statement
Bridge Abutment Stiffness, Design Curves, Soil Behavior	**Unrestricted. This document is available through the National Technical Information Service, Springfield, VA 21161**

19. Security Classif (of this report)	20. Security Classif. (of this page)	21. No. Of Pages	22. Price
Unclassified	**Unclassified**	87	

EXECUTIVE SUMMARY

This report presents an efficient approach to evaluate the nonlinear translational spring stiffnesses to represent seat-type abutments. The applicability of previous studies is limited because such studies are incapable of handling many important factors such as the nonlinear soil behavior, the free-field strains induced by an earthquake, the influence of wing walls, and the difference in soil behavior under active and passive conditions. The proposed approach accounts for all of these factors. The procedures adopted in this approach are relatively simple, and emphasis has been placed on easy interpretation and on achieving consistency between design procedures routinely used in the static and seismic design of abutments. Only routinely used soil properties, such as the relative density, unit weight, angle of internal friction, and interface friction angles, are required in the model.

The proposed approach has been used to develop ready to use design curves to estimate abutment stiffnesses. The design curves have been developed as a function of the height and width of the abutment and the seismic coefficient, k_h (Equation 16). Modification factors have also been developed to account for changes in the baseline parameters used in the development of the design curves (Equation 19). The applicability of the proposed approach has also been verified using recently completed large-scale abutment field tests.

TABLE OF CONTENTS

NONLINEAR BRIDGE ABUTMENT STIFFNESSES: FORMULATION, VERIFICATION, AND DESIGN CURVES

INTRODUCTION

Detailed dynamic response analysis of highway bridges are often required in the seismic safety evaluations of existing structures and new bridge designs. In the case of existing bridge structures, dynamic studies can provide valuable information on the effectiveness of various seismic retrofitting alternatives being considered. Many past earthquakes around the world have clearly demonstrated a significant interaction between the bridge superstructure, abutments, and the approach fill (bridge-abutment-backfill interaction). One of the dramatic consequences of the lack of abutment resistance for longitudinal movement is bridge decks falling off as seen in the well-documented 1971 San Fernando and 1994 Northridge earthquake damage reports. Therefore, one of the very important issues in bridge dynamic analysis is the realistic characterization of bridge-abutment-backfill interaction.

Many experimental and analytical studies have clearly demonstrated that this interaction plays a major role in the overall dynamic behavior of the entire bridge system. Among the experimental studies, work by Douglas and Saiidi (1984), Crouse and coworkers (1987, 1992), Maragakis et al. (1992), and Eberhard et al. (1993) are a few examples of well-documented field tests in which the bridge-abutment-backfill interaction has been addressed. Other system identification studies with measured earthquake response records have also shown that the bridge superstructure-abutment-backfill system significantly interact and that the soil behavior has a first-order effect on the overall dynamic bridge response (Werner et al., 1987, 1990; Wilson and Tan, 1990). In addition, they concluded that, as a result of nonlinear hysteretic

behavior of soils, the earthquake response of especially short-span highway bridges is highly nonlinear. The bridge-abutment-backfill interaction significantly influences the natural period and mode shapes of the bridge system which define the magnitude and distribution of the inertial loads from earthquake excitation (Lam et al., 1991).

The importance of a dynamic analysis that provides allowance for flexibility of the supports at the abutments (as opposed to representing supports at abutments as rigid) has been incorporated into the seismic bridge design guidelines adopted by the American Association of State and Highway Transportation Officials (AASHTO) which had been in use for over a decade (*AASHTO Guide*, 1992). Quite involved and complicated dynamic analysis which integrates extensive seismological and geotechnical input along with the finite element modeling of the entire bridge-abutment-backfill system has been attempted (e.g., Ueng et al., 1994; McCallen and Romstad, 1994); but the adoption of such approaches is unattractive to practicing bridge design engineers.

The finite element (FE) representation of entire bridge-abutment-backfill system results in a significant increase in the problem size and effort of data preparation and interpretation. There are many complicating factors that influence bridge-abutment-backfill interaction. Three-dimensional geometry, nonlinear stress-dependent constitutive relations of soil, and the development of active and passive zones and corresponding slip planes are some of the complex elements that need characterization.

A simpler, economical, and more appealing way to represent the abutments in dynamic response studies is to use translational and rotational springs. Each one of these springs represents the resistance for deformation at the abutment support. Such a representation is very

useful for practicing engineers who can develop a "feel" for the overall bridge response by readily undertaking a parametric study to quantify major contributing abutment interaction factors and their relative importance. Elaborate FE based models often obscure the "physical insight" often needed in making engineering judgment.

Though AASHTO guide specifications recommend that abutments be modeled using equivalent linear spring coefficients in bridge dynamic analyses (*AASHTO Guide*, 1992, section 5-4-2-b), there are no specific recommendations as to how to select the spring coefficients. The current widely used design procedure (e.g., CalTrans) is to perform an iterative elastic analysis until convergence between the assumed and the computed abutment stiffnesses falls within a certain allowable limit. The key element in this procedure is to obtain a realistic engincering estimate of the average stiffness provided by the soil at the bridge abutment. More details on the CalTrans procedure are provided later.

It will be seen from the subsequent section that the current state-of-the-art with respect to the characterization of bridge abutment stiffnesses is not realistic. This may be deduced from the recommendations made in a recent design manual entitled *Manual for Design of Bridge Foundations* (Barker et al., 1991). It states

> "... research is needed to develop better understanding of the behavior of retaining walls and abutments during earthquakes ... These methods should be verified by comparison with behavior of full-scale structures in the field..."

The work described in this report presents a verified realistic procedure to obtain the nonlinear abutment stiffness for bridge seismic response evaluation. It gives a simple analytic model that incorporates all of the important factors that govern abutment stiffness characteristics. Factors such as abutment dimensions, nonlinear stress-dependent soil behavior,

and the strength of excitation are accounted for. Special efforts have been made to insure that the analytical model is simple but yet realistic and requires a very few material parameters that may be obtained from routine, geotechnical tests. The report also describes the results of a verification study undertaken to validate the applicability of the proposed analytical model. Recent large-scale field test results reported by Maroney et al. (1994) have been used in the verification. Finally the report gives ready to use design curves for abutment stiffnesses and describes the application of the proposed procedure.

PROBLEM STATEMENT AND PAST STUDIES

The type of abutments used in a bridge structure depends mainly on the nature of the bridge site, the foundation soil, the bridge span length, and the design load magnitudes. Typical abutment types include free-standing gravity walls, cantilever walls, tied-back walls, and monolithic diaphragms. In the case of seat-type abutments, the bridge deck typically rests on elastomeric bearings mounted on the abutment with a gap of 25 to 75mm provided between the abutment and the deck to allow for thermal expansion. The selection of the abutment type governs the design procedure to be adopted. With respect to design, the abutments may be divided into yielding and nonyielding types. In the case of a yielding type, the abutment is free to yield laterally and may move enough to mobilize the peak (maximum) soil strength in the backfill. On the other hand, in the case of nonyielding abutments, only a partial mobilization of soil strength is present. The current design recommendations provided by AASHTO for yielding and nonyielding types of abutments differ considerably. The objective

of the research work presented here is to develop a simple procedure for representing seat-type abutment stiffness characteristics for highway seismic bridge response studies.

Further, since seat-type abutments are considered, only the characterization of translational stiffnesses (longitudinal, vertical, and transverse) is required. In the case of monolithic abutments, rotational stiffnesses may also have to be characterized in addition to translational stiffnesses.

The abutment is assumed to be founded on a spread footing. Many of the bridges in Nevada with the highest priority for seismic retrofit are on spread footings founded in gravelly and dense sandy soils that have low liquefaction potential. The abutment type considered here represents slightly more than half of the bridges in Nevada.

Figure 1 shows the typical load-displacement characteristics of the longitudinal (or lateral) abutment translation (Lam et al., 1991). Only after the bridge deck movement exceeds the bridge deck-abutment gap distance is there resistance from the bridge abutment. The guidance currently provided by the *CalTrans Bridge Design Aids* recommends a linear elastic behavior for the longitudinal spring until an ultimate load is reached. The recommended value for the initial stiffness is 1.15×10^5 kN/m/m width of the wall (200 kips/in/foot of wall) for typical materials placed at bridge abutments in California. The ultimate abutment load is normally assumed to be limited by a maximum passive soil stress under a dynamic load of 370 kPa (7.7 kips/ft^2). These values are considered appropriate for medium to dense sandy backfill behind a wall of about 2.4m high. The recommended CalTrans procedure is to assign one-half of the abutment stiffness to each abutment at both ends because no or very little soil resistance will be mobilized when the abutment moves away from the soil. (Lam et al., 1991; Werner,

1994). As shown in Fig. 1, the analysis based on an iterative procedure is adopted to model the abutment behavior in a linear elastic dynamic response analysis. It may be noted that, in the CalTrans procedure, the nonlinearity in the abutment stiffness is present because of the abutment-bridge deck gap and passive (ultimate) failure in the soil. Furthermore, the procedure is considered to be applicable only to walls of about 2.4m in height.

Wilson (1988) and Wilson and Tan (1990) developed a stiffness equation for a more general abutment wall-backfill system. For longitudinal stiffness and for transverse stiffness of the wing wall, Wilson (1980) recommended using

$$S_L = \frac{E_s}{(1 - \nu^2) I} \tag{1}$$

in which S_L = the longitudinal abutment stiffness per unit wall width, E_s = Young's modulus, ν = Poisson's ratio of the backfill, and I = the shape factor which depends on the dimensions of the abutment. This equation is based on the vertical displacement of a foundation resting on a uniform elastic half space, and it assumes that soil resistance is identical under compression or tension. Unlike the CalTrans recommendation, the equation above allows for the input of site specific soil parameters and abutment wall dimensions.

There are two serious concerns related to this approach: (1) the applicability of Eq. 1 for problems under longitudinal load applied near the top of the abutment wall and (2) the disregard of the complex interaction of active/passive soil conditions from the soil surrounding the abutment and also of the rotational resistance at the base of the abutment. Furthermore, Wilson's method is linear elastic; and, thus, "a representative" Young's modulus value is needed in Eq. 1. The selection of a single value for use is often quite arbitrary.

Figure 2 shows a sketch of the longitudinal secant stiffness variations given by many researchers. The results are presented in a normalized form in which the stiffness and abutment displacement are normalized with respect to the initial abutment stiffness and the wall height respectively. The influence of the gap between the deck and the abutment has been removed in these plots. This figure is presented to highlight the variation of the secant stiffness with displacement. The results include the following approaches: (1) Wilson, 1980; (2) Maragakis and Siddharthan (1989); and (3) CalTrans with ultimate load limits. In the approach proposed by Maragakis and Siddharthan (1989), the abutment was represented as a thin rigid plate. The soil was assumed to be linear elastic; however, the nonlinearity was present because of failures in the active and passive zones surrounding the abutment. The results from recently completed large-scale abutment filed tests (Maroney et al., 1994) are also provided in Fig. 2. This figure makes it clear that the nonlinear behavior of the abutment was evident in the field test soon after the application of the load; current methods are incapable of representing this response. The inability to represent this response is a consequence of the existing models' inability to characterize nonlinear soil behavior evident even at the low displacement. It may be noted that the field test showed a drop in longitudinal stiffness by as much as eight times when the wall displaced by about 35mm (Maroney et al., 1994). More details on this field testing are provided subsequently.

Many field observations (e.g., downhole array measurements) and seismological data from past earthquakes have revealed that soil exhibits nonlinear behavior in strong motion earthquakes (Yu et al., 1993; Chin and Aki, 1991). An excitation with a maximum acceleration, a_{max}, of around 0.1g is strong enough to require nonlinear characterization of soils

(Chin and Aki, 1991; Finn, 1988). Soil amplification studies are currently routinely carried out using computer programs such as SHAKE (Schnabel, 1972; Idriss and Sun, 1992) and DESRA (Finn, 1988; Lee and Finn, 1991), which model the nonlinear stress-dependent behavior of soil. Therefore, it is imperative, at least for the sake of consistency, that the abutment behavior be modeled using nonlinear stress-dependent material characterization for soil.

In summary, past studies and design procedures that have recommended abutment stiffness values have been based on many assumptions that are not quite realistic. For example, these methods ignore many of the following important factors: nonlinear stress-dependent soil behavior, earthquake induced strains (i.e., free-field strains), the influence of the strength of the base excitation, the presence of active and passive conditions and the corresponding difference in soil behavior under such conditions, the influence of wing walls, and the physical abutment dimensions (Tsai et al., 1993; Werner, 1994). The nonlinear abutment stiffness procedure presented below is based on a number of well-established concepts that are routinely used in soil mechanics. The proposed procedure is simple and accounts for all of the important factors identified above.

PROPOSED MODEL

The objective of this study is to propose a simple method for representing longitudinal, vertical, and transverse load-displacement characteristics of seat-type abutment systems resting on spread footings. For such abutment types, only the translational behavior of the abutment at the extreme ends of the bridge deck axis, which is often near the top of the abutment, must

be defined. Figure 3 shows the longitudinal spring (S_L), vertical spring (S_V), and translational spring (S_T) connected to the deck. It should be noted that the springs will become effective only after the deck-abutment gap has been closed. Any one of the load-displacement relationships can be evaluated by estimating the force required to cause a given displacement. The development of longitudinal spring stiffness characteristics is presented first.

I. Longitudinal Abutment Stiffness (S_L) Evaluation

Figure 4 shows a sketch of a displaced abutment caused by a horizontal longitudinal force, P_L, applied at the abutment-bridge deck support. Abutment longitudinal displacement near the top is δ_L, and it rotates through θ as shown. The movement of the abutment suggests that active and passive conditions can develop in front and at the back of the abutment as shown. At the bottom of the abutment, there is resistance for rotation resulting in an increase or decrease in foundation pressures as shown in the figure. A close look at the figure suggests that, to estimate the force P_L for a given displacement δ_L, one is required to characterize (1) the lateral wall movement-earth pressure relationship under active and passive conditions and (2) the interaction between the abutment base and the foundation soil. Procedures adopted to establish these relationships are presented below.

Lateral Movement-Earth Pressure Relationship

The lateral earth pressure that acts on a wall varies with the wall displacement. When the wall moves away from the backfill, the earth pressure decreases (active pressure); and, when it moves toward the backfill, the earth pressure increases (passive pressure). Laboratory measurements and finite element studies (Clough and Duncan, 1991; Barker et al., 1991) have

shown that (1) the active conditions in a soil deposit can be mobilized with a much lower wall movement than the passive conditions and (2) the normalized wall movements (Δ/h), specified as a fraction of the wall height, h, can be used to represent the relationship between the wall movement and lateral pressure. This relationship is applicable for the sliding and tilting movements of the abutment. Figure 5 presents a range for lateral earth pressure-wall movement relationships reported for compacted and uncompacted medium dense sand. The vertical axis has also been normalized with respect to active and passive coefficients of earth pressure. It is seen from the figure that, for medium dense sand, the Δ/h ratio for the passive mobilization is as much as ten times that needed for active mobilization. The average curve shown in Fig. 5 was selected to represent the active and passive pressure-wall displacement relationship in the proposed model.

Resistance for Deformation at Abutment Base

The abutment base undergoes vertical and lateral movements and rotation. The resistance at the base is defined by a vertical reaction, F_v, resistance in the horizontal direction, F_h, and resistive movement, M_b (Fig. 4). Since the resisting moment is a result of changes in vertical resistance at the base of the abutment, the resistances for vertical movement and rotation are interconnected. Using a Winkler spring representation for the foundation soil, Siddharthan et al. (1992) developed a rational procedure to obtain the resisting moment, M_b, versus rotation, θ_b, relationship. They considered two important aspects: the foundation pressure should not exceed the ultimate bearing capacity and possible lifting off of the foundation.

Figure 6 shows a simple foundation model of width B supporting a vertical force, F_v (per unit width) resting on Winkler springs that are not bonded to the foundation. As the value of the moment, M_b, steadily increases, the stresses in the foundation springs to the right increase while there is a reduction in the stresses in the springs on the left of center. Siddharthan et al. (1992) showed that, depending on the value of F_v, the foundation could first reach ultimate bearing capacity (right corner) and then subsequently lift off (Case A) or vice versa (Case B). Case A occurs when $F_v \geq q_{ult}B/2$ in which q_{ult} is the bearing capacity of the foundation soil. In this case, until ultimate bearing capacity is reached, the moment-rotation (M_b-θ_b) relationship is linear and is given by

$$M_b = \frac{k_v B^3}{12}\theta_b \qquad for \qquad 0 \leq \theta_b \leq \theta_{bm} \tag{2}$$

in which $\theta_{bm} = 12M_{bm}/(k_vB^3)$,

$$M_{bm} = \left[q_{ult} - \frac{F_v}{B}\right]\frac{B^2}{6} \tag{3}$$

and k_v = the coefficient of subgrade reaction. For $\theta_{bm} \leq \theta_b \leq \theta_{bl}$, the moment-rotation relationship is nonlinear and given by

$$M_b = 3M_{bm} - \sqrt{\frac{48M_{bm}^3}{k_vB^3\theta_b}} \qquad for \qquad \theta_{bm} \leq \theta_b \leq \theta_{bl} \tag{4}$$

in which θ_{bl} is the value of θ_b when lift off is initiated at the left corner. Here θ_{bl} is given by

$$\theta_{bl} = \frac{q_{ult}^2 B}{12k_vM_{bm}} \tag{5}$$

For a further increase in M_b (i.e., $\theta_b > \theta_{bl}$), Siddharthan et al. (1992) proposed using an ultimate moment resistance given by

$$M_b = 3M_{bm} - \frac{24M_{bm}^2}{q_{ult}B^2} \quad (6)$$

A similar approach to generate the M_b - θ_b relationship for Case B has also been provided by Siddharthan et al. (1992), and their results for both Cases A and B are summarized in Fig. 7.

Coefficient of Subgrade Reaction, k_v

One of the important input parameters required to use the equations shown in Fig. 7 is k_v. The approach proposed to obtain k_v is based on Schmertmann's (1978) strain factor method which is a widely recommended procedure in many design manuals for estimating settlements of footings in sand (*Engineering Manual*, 1990; Barker et al., 1991). This method provides a logical means of accounting for the variations in the stress-dependent nonlinear stiffness of sand with depth. The analysis is based on the assumption that the distribution of vertical strain below the footing is compatible with linear elastic half space. Its applicability has been verified using the finite element studies and many field and laboratory observations (Schmertmann, 1970; Schmertmann et al., 1978). According to Schmertmann's method, the settlement, δ_v, of a uniformly loaded surface footing can be written as

$$\delta_v = C_p \sum \epsilon_v \Delta z = C_p \sum \left[\frac{\Delta p I_z}{2B(1+\nu)G}\right]\Delta z \quad (7)$$

in which ε_v = the vertical strain in the sublayer in the foundation soil, C_p = the correction factor, Δp = the net applied footing pressure given by (F_v/B - σ_o), σ_o = the overburden pressure at the base of the foundation, Δz = the thickness of the sublayer, I_z = the vertical strain influence factor, and G = the secant shear modulus of the sublayer. Other terms have been

defined previously. An iterative procedure adopted to account for the stress-dependent nonlinear foundation soil is presented below.

(1) Divide the soil beneath the foundation into a number of sublayers up to about four times the width of B (Fig. 8a) and assume a certain value of F_v.

(2) For each layer, assume the initial secant shear modulus, G, to be a fraction of G_{max}. Here, G_{max} is the maximum shear modulus at a low shear strain; and it may be computed using the Seed and Idriss (1970) equation

$$G_{max} = 218.8(K_2)_{max}(\sigma_m)^{\frac{1}{2}} \qquad (8)$$

in which $(K_2)_{max}$ = the constant that depends on the relative density of the soil and σ_m = the mean normal stress of the layer. Here, G_{max} and σ_m are given in kPa and σ_m is computed using both components: the overburden and the load induced stresses. The average load induced stresses in the sublayer were computed using a 2:1 spread as often used in foundation engineering.

(3) Compute the vertical strain, ε_v, in each sublayer using the terms that are within the brackets in Eq. 7. The variation of I_z is shown in Fig. 8b.

(4) Estimate the average shear strain, γ_{ave}, in the sublayer using Seed (1983)

$$\gamma_{ave} = (1 + \nu)\,\epsilon_v \qquad (9)$$

and the shear modulus given for this shear strain from the shear modulus reduction curve of Seed and Idriss (1970) shown in Fig. 9.

(5) If the difference between the assumed (Step 2) and the computed (Step 4) shear modulus is not within a certain limit, repeat Steps 2 through 4. If convergence occurs in all sublayers, then compute the foundation settlement, δ_v, using Eq. 7.

The entire nonlinear vertical load-settlement (F_v versus δ_v) curve can be obtained by increasing the value of F_v. The curve is limited by the ultimate bearing capacity of the foundation as shown in Fig. 9. The secant subgrade reaction, k_v, can be estimated for any given vertical load, F_v, as shown in the figure.

Horizontal Force (F_h) - Displacement (δ_h) Relationship at the Base

A similar procedure to the one described above has been adopted to arrive at the F_h-δ_h relationship. The lateral movement, δ_h, is given by

$$\delta_h = \sum \gamma_h \Delta z = \sum \left[\frac{F_h I_h}{BG}\right] \Delta z \qquad (10)$$

in which γ_h = the shear strain in the sublayer and I_h = the shear strain influence factor. The shear strain influence factor, which is similar to Schmertmann's vertical strain influence factor, has been deduced from the elastic half space solution (Schmertmann, 1978; Poulos and Davis, 1974). The iterative procedure outlined above has again been adopted to arrive at the nonlinear F_h-δ_h relationship. The limit to this relationship is imposed by the interface friction force given by $F_v \tan\delta_f$ in which δ_f is the interface friction angle between the foundation soil and the base.

Equilibrium of Displaced Abutment

Figure 11a shows the typical boundary forces and moments surrounding the abutment (also see Fig. 4). The lateral stress at any point located in the front and back of the abutment is computed by multiplying the lateral pressure coefficient, k, from Fig. 5 by the vertical stress at that point. The net force on the wall is the integration of this stress over the height of the abutment. For example, the lateral force P_1 shown in Fig. 11 is

$$P_1 = \frac{1}{2} k\gamma H^2 \qquad (11)$$

in which H = the height of the passive zone in front of the abutment and γ = the unit weight of the soil. This force is at an angle δ_b, which is the angle of friction at the vertical slip plane. Since the abutment undergoes rigid body movement, it is possible to evaluate the abutment displacement at any point in terms of δ_L and θ. Using the abutment displacement, the coefficient k can be obtained from Fig. 5. The lateral passive and active earth pressure coefficients, K_p and K_a, required to carry out these calculations may be obtained from Coulomb equations. As recommended in the recent design manual (Barker et al., 1991), the Coulomb coefficient, K_p, has been modified to account for a more realistic failure surface. This modification substantially reduces Coulomb's value. In the case of the lateral resistance at the base of the abutment, the displacement at the center of the base is used.

It is necessary to find P_L for a given displacement, δ_L, near the top of the abutment (Fig. 4) such that force and moment equilibrium equations are simultaneously satisfied. A simplified step-by-step procedure adopted to achieve this condition is as follows.

(1) Assume a certain small starting value for δ_L, and increase the wall rotation, θ from zero.

(2) For the assumed value of θ, compute the lateral wall forces, P_1 and P_2, the base resisting moment, M_b, and the lateral base resistance, F_h.

(3) Use the horizontal equilibrium condition to get an estimate of the force P_L.

(4) Check for moment equilibrium by taking moments about the center of the abutment base. If the net (or residual) moment changes signs between two subsequent θ values, then the moment equilibrium is satisfied between these two values. If the net moment does not change sign, repeat the procedure from Step 2 with an increased value of θ.

(5) Repeat Steps 1 through 4 for the next δ_L value.

It has been found that the proposed iterative procedure converges very quickly. The nonlinear longitudinal secant spring stiffness, S_L, is subsequently computed using $S_L = P_L/\delta_L$.

Earthquake Induced Inertia Forces and Free-Field Strains

The earthquake excitation shakes the bridge superstructure and also foundation and backfill soil surrounding the abutment. It may be argued that the strains in the surrounding soil have two components: free-field and strains from load applied at the abutment. This means that, since the soil is nonlinear, it is reasonable to expect that the abutment stiffness depends on the level of shaking. Since the dynamic characteristics of the superstructure and soil surrounding the abutment are quite different, the movement of the soil adjacent to the abutment will not be in phase with the bridge deck movement. When the bridge attempts to push into the abutment, there may be inertia forces present within the backfill and on the abutment. The analysis presented thus far neglects the influence of the inertia force. In fact, all of the current methods neglect the presence of inertia force. When inertia force is present, the maximum active and passive resistances for lateral movement are given by the Mononobe-Okabe equation (Seed and Whitman, 1970). Since the lateral earth pressure versus displacement curve adopted here is normalized, Mononobe-Okabe active (K_{AE}) and passive coefficients (K_{PE}) can be used with Fig. 5.

Since the excitation reverses in direction very often, the horizontal inertia forces could be in a direction either to the left or to the right or even nonexistent when the deck attempts to move into the abutment. A similar situation exists with the vertical inertia force. Under

these circumstances, it is herein proposed to evaluate abutment stiffnesses considering many possible combinations. The combinations that have been considered are horizontal seismic coefficient $k_h = \pm 0.5\ a_{max}/g$, the vertical seismic coefficient $k_v = \pm k_h/2$, and also $k_h = k_v = 0$. Here, a_{max} is the maximum horizontal acceleration on top of the soil deposit and k_v has been assumed to be half of k_h. The selection of values for the seismic coefficient, k_h, had been based on the recommendation of Whitman (1991) who critically reviewed field observations in real earthquakes and laboratory tests. Altogether, there are five combinations; and, since the problem is nonlinear, it is not possible to predict beforehand which combination would yield the conservative results. It is believed that the cases with inertia forces and free-field strains and the case without earthquake excitation (k_v=k_h =0) can provide a bound for the stiffness evaluations.

The foundation and the backfill soil mass undergo deformation to the earthquake excitation (free-field). The free-field strains that are present due to earthquake shaking should be superimposed on the load induced strains for realistic nonlinear characterization (Lam and Martin, 1987; Buckle et al., 1987). The steps taken to incorporate earthquake induced inertia forces and free-field strains are as follows.

(1) Compute the average free-field shear strains, γ_{eq}, in the foundation and backfill soil as a function of depth using the procedures outlined by Tokimatsu and Seed (1987). This approach requires widely used soil properties such as $(K_2)_{max}$, and unit weight, a_{max}.

(2) Superimpose the γ_{eq} on the load induced shear strain, γ_{ave}, computed in Eq. 9 using

$$\gamma_{total} = \sqrt{\gamma_{eq}^2 + \gamma_{ave}^2} \qquad (12)$$

in which γ_{total} is the net strain. Use γ_{total} in the development of the F_v versus δ_v relationship. Since both of the shear strain components are on two different perpendicular axes, they have not simply been added. Further, when inertia forces are considered, the bearing capacity of the foundation is reduced. Recent research reported by Richard et al. (1993) has been used to obtain the limit to the F_v versus δ_v relationship (Fig. 9) as a function of the strength of design excitation defined by $k_h = 0.5\ a_{max}/g$.

(3) In the development of the F_h versus δ_h relationship, the net shear strain, γ_{total}, is obtained by adding both components, γ_h and γ_{eq}. Subsequently, γ_{total} is used to obtain the secant shear modulus from Fig. 9.

(4) In the development of the lateral earth pressure-displacement relationship using Fig. 5, the net stress strain, γ_{total}, estimated from

$$\gamma_{total} = \left(\frac{\Delta}{h}\right)_{total} = \left(\frac{\Delta}{h}\right) + \gamma_{eq} \qquad (13)$$

is used to obtain the lateral earth pressure.

(5) Finally, as before, use boundary forces and moments surrounding the abutment shown in Fig. 11b to compute the force P_L required to cause a selected longitudinal deformation, δ_L.

The procedure used in the computation of net strains is consistent with those adopted in the structural response evaluation of a multi-modal system from a response spectrum.

II. Vertical Abutment Stiffness (S_V) Evaluation

Figure 12 shows a sketch of a displaced abutment caused by a vertical force, P_V, applied at the abutment-bridge deck support. The abutment undergoes a vertical movement, δ_V, at the support as shown. The figure also shows active and passive zones surrounding the abutment. It is evident that the estimation of the vertical force, P_V, can be made using the same procedures proposed above for estimating the lateral force.

Though the figure shows the abutment rotating clockwise, the real direction of rotation is not known. The direction of rotation will depend on base and lateral resistance on the boundary. The procedure that was adopted here assumes that initially the abutment rotates clockwise and then counterclockwise for the given δ_V. The lower value of the force is only used to calculate the vertical stiffness, S_V. It has been observed that, once the abutment rotates in one direction, it continues to rotate further in the same direction as the abutment displacement, δ_V, is increased.

III. Transverse Abutment Stiffness (S_T) Evaluation

Figure 13 shows an abutment displaced transversely through a displacement δ_T when applied with a force P_T. The wing walls, which are often provided to retain soil near the abutment, play a major role in providing resistance. Typically, only a part of the outer wing wall face is buried in the soil. However, the entire internal faces are buried. The displacement mechanism shown in Fig. 13 identifies the active and passive zones. Opposing types of failure zones exist across a wing wall. The resistances derived from these failure zones can be obtained from the procedures outlined above. The portion of the wing wall buried in the soil

varies with depth (see Fig. 3). Therefore, the resistance on the wing wall is computed using a number of small horizontal strips of varying widths. There is an additional component of resistance for deformation present on the back of the abutment. The figure shows this force as T_T.

If the wing walls lie close to each other, substantial overlap can occur between the failure zones in the soil confined within the wing walls. Under these conditions, the active and passive force-displacement relationship may not fully develop as shown in Fig. 5. In such cases, it is necessary to reduce the lateral resistance to account for overlapping. Figure 14 presents a simplified procedure to achieve this. In the case shown in Fig. 14a, no overlap exists. Here, α_a and α_p represent the inclination of failure planes for the active and passive zones respectively. Similarly, d_a and d_p represent the corresponding thicknesses of the zones. In the case depicted in Fig. 14b, an overlap occurs within the hatched region and full resistance within this region will not be mobilized. By neglecting resistance within the hatched region, it is possible to show from first principles that the ultimate pressures on the wing wall can be computed by modifying the passive and active earth pressure as

$$\left(P_a\right)_{overlap} = \left(P_a\right)_{\substack{without\\overlap}} \left[\frac{d_a^2 - d_o^2}{d_a^2}\right] \qquad \textbf{(14a)}$$

and

$$\left(P_p\right)_{overlap} = \left(P_p\right)_{\substack{without\\overlap}} \left[\frac{d_p^2 - d_o^2}{d_p^2}\right] \qquad \textbf{(14b)}$$

in which d_o = the thickness of the overlapping region (Fig. 14b). Our calculations show that the influence of overlapping is evident only for taller abutments (more than 5m) supporting two

or fewer lanes. In other cases, the overlapping is minimal and can be neglected. Under an extreme case of a taller abutment with less than two lanes, the entire passive zone may not be able to be accommodated within the soil confined between the wing wall. In such cases, the entire soil mass within the wing wall along with the abutment can behave like a single rigid body. This case is then very similar to the longitudinal deformation analysis presented above.

The number of lanes supported by the abutment dictates the abutment width, W, in the transverse direction. For a two-lane highway, the width is typically 10m. Since this is quite wide and the interface extends to the entire height of the abutment, the resistance (T_T) at the interface between the backfill and the abutment is an important resistance component. Though the interface force-displacement relationship (F_h-δ_h) developed earlier for the abutment base can be used here, the face of the abutment should be subdivided for better accuracy because the resistance within the interface cannot be assumed to be uniform. Unlike in the case of interface resistance at the base of the abutment, a much larger interface is involved in providing resistance for the transverse deformation. The maximum interface resistance that can be mobilized at any point on the interface depends on the depth from the surface of that point. The procedure adopted here first divides the interface into a number of smaller rectangles as shown in Fig. 15 and then evaluates the resistance for transverse deformation at the center of these rectangles. It may be noted that the resistance in each rectangle has two components: a horizontal and a vertical. This is because the rectangle undergoes movement in both directions for the deformation mechanism assumed in Fig. 13.

The final task in the computation of the transverse stiffness is to undertake a similar iterative procedure as described previously to find P_T such that all equations of equilibrium are

satisfied. It should be noted that the major contributing component is the resistance for rotation provided at the base of a foundation of a much wider foundation width.

NUMERICAL EXAMPLE

To illustrate and highlight many important components of the proposed approach, many intermediate steps involved in the evaluation of the nonlinear stiffness of an abutment shown in Fig. 16 are presented. This is a medium high abutment with a height of H = 4.5m supporting a vertical deck load of V_D = 500 kN/m. This abutment has been designed according to the current design procedures (Barker et al., 1991; NAVFAC, 1982) such that the factors of safety under static loading conditions against sliding, overturning, and bearing failures are more than 1.5, 2.0, and 2.0 respectively. Tension at the heel of the abutment is also not allowed to develop. In addition, this abutment has factors of safety under seismic loading conditions against sliding, overturning, and bearing failure of more than 1.1, 1.5, and 1.5 respectively. These factors of safety are consistent with those recommended in various design guidelines for abutment design (e.g., Barker et al., 1991; NAVFAC, 1982; Siddharthan et al., 1994). A seismic coefficient, k_h = 0.2 and k_v = 0.1, has been used in the pseudostatic design of the abutment. The backfill and foundation soil are assumed to have a friction angle of $\phi_b = \phi_f = 35°$, and the interface friction angles at the base and on the side are assumed to be 21° and 15° respectively. These values are typical for medium dense sand and sandy silt mixtures (Barker et al., 1991; NAVFAC, 1982). An optimization technique described by Siddharthan et al. (1994) was used to arrive at the abutment dimension at the base of the footing. Table

1 gives the abutment dimensions, deck loads, soil properties, and factors of safety against all failure modes for this abutment.

Figure 17 shows the vertical load-displacement (F_v - δ_v) relationship obtained for this abutment. Two cases are shown: (1) $k_h = k_v = 0.0$ and (2) $k_h = 0.2$ and $k_v = 0.1$. The limiting vertical load given by the bearing capacity equations with $k_h = 0.2$ is much smaller and is as much as 0.3 of the limiting vertical load when $k_h = 0$. The F_v-δ_v relationship developed for $k_h = 0.2$ required a knowledge of free-field strains. The procedures adopted by Tokimatsu and Seed (1987) were used to estimate the average free-field shear strains. Figure 18 presents this variation. These strains were superimposed with the load induced strains, as in Eq. 12, to obtain the F_v-δ_v relationship for the case where $k_h = 0.2$. It may be noted that the nonlinear behavior is present from the start and the ultimate bearing pressures is reached in the cases of $k_h = 0.2$ much sooner after the vertical displacement of 7mm; while, in the case of $k_h = 0.0$, as much as 62mm displacement is required. It appears that there is no major difference between the cases $k_h = 0$ and $k_h = 0.2$ until the ultimate bearing resistance is reached with the $k_h = 0.2$ case.

Figure 19 shows the horizontal load-displacement (F_h-δ_h) relationship at the abutment base for both the cases. Unlike in the case of the F_v-δ_v relationship, there is significant deviation between the curves shown in Fig. 19. The figure also shows an arbitrary cutoff limit to illustrate that the strength at the interface, given by $F_v \tan\delta_f$, governs the maximum value of F_h. The value of F_v varies during the abutment movement, and it has to be evaluated by resolving the forces shown in Figs. 11a and 11b in the vertical direction. It may also be noted

that, unlike in the case of the F_v-δ_v relationship, the mobilization of the horizontal resistance is much more quickly achieved.

Figures 20a, 20b, and 20c respectively present the longitudinal, vertical, and transverse stiffnesses evaluated using the procedures outlined above. Each of these figures depicts five cases. As described above, when inertia forces are considered, four cases are necessary to cover the variations in the direction of the horizontal and vertical inertia forces. The fifth case is with $k_h = k_v = 0$. In all of the cases reported in the figures, it is clear that the stiffness drops substantially, by as much as a factor of 9, when the displacement increases from 1 to 10mm. For all cases, after about 20mm of movement, there is not much change in the stiffness. Figures 20a, b, and c show the range of stiffnesses. The case of $k_h = 0.2$ and $k_v = 0.1$ always represents the upper bound (stiffer) data, while the case of $k_h = k_v = 0$ represents the lower bound (softer) data. The highest deviation between the five cases exists at a lower displacement; and it can be as much as 40%, which occurs in the case of vertical stiffness. The differences in S_L, S_V, and S_T between the five cases at 1mm of displacement are about 18%, 40%, and 25%. The value of S_V is much larger than S_L and S_T as has often been observed in system identification studies based on responses measured in an earthquake and from quick-release tests (Wilson and Tan, 1990; Werner et al., 1990).

In design, it is often customary to select the lower abutment stiffnesses. This is because lower abutment stiffnesses will usually produce higher displacements for the deck and the pier and, therefore, lead to higher ductile demand and shear forces in the pier. However, in an extreme case when an iterative elastic bridge response analysis is performed, the softer springs can change the dynamic characteristics (period and mode shapes) and, thus, result in an

unrealistic analytical model. Since the variations shown between the different cases are within 40%, the influence of this on altering the effective period of the entire bridge structure will be minimal.

FIELD VERIFICATION

Large-scale field verification, though expensive, may be warranted for the validation of geotechnical engineering models, especially when nonlinear stress-dependent soil behavior is a governing factor. A physical model acts as an analog that automatically accounts for various mechanisms that interact to produce the overall response. Laboratory centrifuge is another valuable technique that is becoming widely used by the engineering community to study geotechnical problems involving nonlinear stress-dependent soil behavior (Finn, 1988; Arulanandan and Scott, 1994). The verification study reported here used abutment field test results recently reported by Maroney et al. (1994)

Brief Description of Field Tests

Maroney et al. (1994) provided a detailed description of a well-instrumented testing program undertaken for CalTrans to characterize abutment behavior. They tested to failure two large-scale abutments 1.7m and 2.1m high. While the taller (east) abutment was tested in the longitudinal and transverse directions, the shorter (west) abutment was tested only in the longitudinal direction. Both abutments were founded on 230mm cast-in-drilled-hole (CIDH) piles and provided with wing walls as shown in Fig. 21. The east abutment sat on four piles, while the west abutment sat on three. The figure shows plan and elevation views of the two abutments and the loading directions. The west abutment supported an embankment constructed with a low plastic clayey silt (Yolo loam) having a PL of 23.5 and a PI of 10.5. Maroney et al. (1994) suggested that the clayey silt exhibited substantial cohesive behavior. The eastern embankment consisted of poorly graded coarse clean sand compacted at 90% relative compaction, and its friction angle is estimated to be about 40°. These two materials are considered to represent the type of materials used in approach fill construction in California.

Cone penetration tests (CPT) conducted at the site prior to abutment construction indicated that the upper 5.5m of soil consists of silty sand to sandy silt underlined by a 1.8- to 3.0-m thick layer of clayey soil followed by silty sand to sandy silt at greater depths. The water table was 9.1m from the surface.

In the first phase of the field testing, the abutments were pushed against each other (longitudinal testing) without reaching failure; subsequently, the taller east abutment was loaded transversely to failure. Finally, the shorter west abutment was loaded to failure in the

longitudinal direction using the taller east abutment as a support. In the longitudinal test, the maximum west abutment displacement was as much as 180mm; and, in the transverse test, the east abutment displaced by about 105mm. This testing setup resulted in two longitudinal load responses against two different embankment materials (clayey silt and clean sand) and in one transverse load response against a clean sand embankment. Two 1800 kN hydraulic rams were used to apply the loads to the abutments as shown in the figure. The transverse test on the taller abutment required a reaction frame; and a frame consisting of two, 1.2-m diameter drilled shafts was used. In the longitudinal tests, the loads were applied at mid height on the abutments; while, in the transverse test, the load was applied near the top.

The loads against the abutments were applied in a cyclic manner with a steadily increasing magnitude. The entire testing was instrumented with an extensive network of pressure transducers, magnerules, LVDTs, strain gages, and inclinometers. As many as nineteen pressure transducers cast into the abutment measured soil pressures against the abutment and wing walls. As many as 100 strain gages were placed on the abutment piles. A collection of 20 magnerules and LVDTs monitored the abutment displacements. Since the approach to be verified is for granular material, only the results pertaining to the east abutment are presented below. For more detail on the instrumentation and testing program, see Maroney et al. (1994). The test results represent a unique situation in which extensively instrumented large-scale wall abutments were tested to failure in the field.

Figure 22 shows the longitudinal and transverse secant abutment stiffnesses of the east abutment as a function of abutment displacement. It is clear from the figure that the abutment behavior is nonlinear right from the start of the test. The longitudinal stiffness at a low

displacement (around 1mm) was measured to be around 1.24 x 10^5 kN/m, and it dropped by as much as a factor of 3.7 when the displacement increased to 32mm. The longitudinal test was not continued further. On the other hand in the case of the transverse test, the stiffness around 1mm was about 8.9 x 10^4 kN/m and it dropped to 8.8 x 10^3 kN/m at a displacement of 105mm. The reduction in stiffness is by as much as ten. The transverse test was continued until the abutment failure was clearly evident.

The test results reported above are for an abutment with piles. Maroney et al. (1994) subtracted the lateral resistance contribution from the piles and provided the secant stiffnesses computed only from the resistance offered by the abutment. They presented the contribution from the abutment only for the case of the west abutment which supported the clayey silt embankment. Since the approach being considered here is for sandy soils (noncohesive), the results reported in Fig. 22 for the sandy embankment (east abutment) has to be modified to reflect the stiffness contribution from the abutment only. This was achieved by assuming that the contribution from the piles in the case of the east abutment is 4/3 times the contribution from the west abutment. This is because the east and west abutments are on four and three piles respectively. Figures 23a and 23b present the modified field secant abutment stiffnesses along with those predicted. As reported in the field test, the longitudinal load was applied at mid depth while the transverse load was applied at 0.20m from the top of the abutment. The stiffnesses have been divided by the width of the wall in the transverse direction (4.73m) and presented in terms of kN/m/m of the wall width. The soil properties used with the proposed approach were either reported by Maroney et al. (1994) or interpreted from design manuals (NAVFAC, 1982; Barker et al., 1991). Table 2 gives the values used for the soil properties.

The interface friction angles at the base and on the side of the abutment were selected to be 21° and 15°. These are consistent with values recommended for use for concrete cast on clayey silt soils and side friction against clean medium dense sand. The relative compaction in the embankment is reported to be 90%, which is assumed to represent a relative density of about 70% (Byrne, 1987). Figure 24 shows the abutment dimensions used to evaluate the abutment stiffnesses.

The comparison between the predicted and reported stiffness values is excellent. In the case of a longitudinal abutment (Fig. 23a), there is a slight overprediction at the low displacement of about 10%, which is well within the variation accepted in geotechnical engineering design. At other levels of displacement, the predicted longitudinal is slightly lower. A similar overprediction is also seen in the case of transverse stiffness (Fig. 23b). However, overall, the agreement between the predicted and computed stiffnesses is excellent.

The field testing program described by Maroney et al. (1994) also investigated the failure surface developed behind the abutment using foam columns. They reported that the failure surfaces developed behind the abutment was consistent with passive failure zones, and that the abutment movement was rigid body movement. These findings support and lend credibility to the assumptions used in the development of the proposed approach.

DEVELOPMENT OF DESIGN CURVES

To evaluate the abutment stiffnesses, the dimensions of the abutment must be known a priori. Since nonlinear characterization is used for soil, the strength of the excitation is also required. Figure 25 shows a typical seat-type abutment along with various dimensions that

define the abutment. For transverse stiffness evaluation, the wing wall dimensions are required; the figure also defines these. The abutment should be designed based on its height and also on the strength of excitation in the dynamic design of the abutment. This means that, for a given abutment height, there are many abutments with different dimensions depending on the level of excitation used in the dynamic design.

The dimensions, A_2 and A_3 shown in Fig. 25, are typically governed by seating width and deck thickness requirements (see *AASHTO Guidelines*, 1992). Siddharthan et al. (1994) argued that the heel and toe projections at the base (A_5 and A_6 respectively) are the two dimensions that may be considered as independent variables in the foundation design of the abutments. Using this interpretation, they developed an optimum design procedure to estimate the dimensions A_5 and A_6 such that these are appropriate factors of safety against all possible static and pseudostatic (dynamic) failure conditions. Table 3 shows the factors of safety selected from various design manuals for static and pseudostatic (dynamic) loading conditions.

The factors of safety under the seismic loading condition are smaller to account for the fact that the seismic loading is transient (Whitman, 1991). Note that the factors of safety under seismic loading are assumed to be 75% of the corresponding values under static loading (Seismic, 1990; Gantes et al., 1989). The horizontal seismic coefficient, k_h, that should be used in the pseudostatic analysis should be much smaller than a_{max}, which is the maximum acceleration on top of the soil deposit. A seismic coefficient, k_h, of 0.333 to 0.5 a_{max}/g has been suggested by Whitman (1990); and a value of 0.5 a_{max}/g has been used here.

The optimum design procedure was used to arrive at the abutment dimensions A_5 and A_6 for three abutment heights H = 2.5, 4.5, and 6.5m at three levels of earthquake excitation given by a_{max} = 0.1g, 0.3g, and 0.5g. In the seismic loading conditions, the vertical seismic coefficient was assumed to be $k_v = k_h/2$. The soil properties, which were presented in Table 2 and used in the validation study were also used in the development of the design curves. The vertical and horizontal deck forces, V_D and H_D have been assumed to be 250 and 100 kN/m. Table 4 shows the dimensions of nine abutments obtained based on the optimum design procedure of Siddharthan et al. (1994). These abutments represent three abutment heights and three levels of excitation. Factors of safety under seismic loading conditions have only been shown because these are the critical values that affected the abutment design. In all cases, the static factors of safety fell well above those shown in Table 3.

Figures 26a, 26b, and 26c show the secant abutment stiffnesses in the longitudinal (S_L), vertical (S_V), and transverse (S_T) directions for the three abutments considered in the study. All of the translational stiffnesses are presented as per unit width of the abutment in the translational direction (W). Since the intention is to show the trends, the figures show only the results for the case of k_h = 0.15 and k_v = 0.075 (see Walls 2, 5, and 8 in Table 4). When the deck attempts to push into the abutment, substantial inertial force may be present in the backfill and on the abutment. The abutment translational springs will be engaged many times during the base excitation; and, in all likelihood, the abutment movements and the bridge deck movements will not be in phase. The direction of the inertia forces in relation to the deck movement cannot possibly be predicted. Therefore, four combinations for the inertia forces on the abutments and the backfill were considered between $k_h = \pm a_{max}/2g$ and $k_v = \pm k_h/2$.

This report presents only the softest stiffness because the softer stiffness values will, in general, produce a conservative design for the deck movement and foundation pier. The relative differences between all four cases have been discussed previously.

The variation, S_L (Fig. 26a), between all the abutments is very similar except at low abutment displacement; the taller abutment (H = 6.5m) shows a somewhat higher stiffness of as much as 13% above the stiffnesses of the other abutments. At larger displacements, the abutment stiffnesses are independent of height and are virtually identical. A comparison of the results shown in Fig. 26a with the field data reported in Fig. 23a reveals that the rate of change in longitudinal secant stiffness within the first 10mm is much quicker in Fig. 26a. There are two important reasons for this behavior. Firstly, the longitudinal load was applied at the middle of the abutment in the field test; whereas, in the computed results, it was applied more realistically near the top of the abutment. Secondly, the computed results shown in Fig. 26a have the influence of the vertical and horizontal deck loads (V_D and H_D). The presence of deck forces significantly influence the equilibrium equations that are being solved.

It is often customary to use a "normalized" stiffness, S_L, curve from which stiffness values for other abutment sizes can be scaled. The "normalized" stiffness S_L is often given for an abutment of height 2.4m (8 feet) since this represents a typical abutment. The scaling to other size abutments is carried out assuming S_L is proportional to abutment height (Lam et al., 1991; Maroney et al., 1994, Werner, 1994). This is assumed to be true even though the abutment base widths will differ for abutments with different heights. Figure 26a clearly demonstrates that such an assumption is incorrect and can lead to an erroneous estimate for abutment stiffness.

There is a substantial difference between the stiffnesses of abutments in the case of S_V (Fig. 26b). The taller abutment shows a much higher stiffness due, in part, to the larger width at the base. The widths at the base for the abutments (B) with H = 2.5, 4.5, and 6.5m are 2.15, 2.4, and 3.10m respectively (see Table 4). In the case of transverse stiffness, the difference between the taller abutments (H = 4.5 and 6.5m) is minimal while the shortest abutment (H = 2.5m) shows a much lower stiffness.

To demonstrate a typical trend, the longitudinal stiffness, S_L, variation shown in Fig. 26a has been replotted in log-log scale along with best-fit straight lines in Fig. 27. The data shows that the S_L variation with displacement in the log-log plot can be assumed to be linear. It has been observed that all of the translational stiffnesses demonstrated the same characteristics. To verify whether the large-scale field tests detailed above also showed the same trend, all available large-scale abutment field data of Maroney et al. (1994) are plotted in log-log scale in Fig. 28. There are two longitudinal stiffness plots, representing the east and west abutments, and one transverse stiffness plot for the east abutment. It should be noted that the stiffness contribution from only the abutments are presented. This plot also verifies, for practical purposes, the variation of translational stiffnesses can be assumed to be on straight lines in a log-log plot. This means that the variation of any translational secant stiffness can be written as

$$S_i = S_{oi} x_i^{-\lambda} \qquad (15)$$

in which S_i = the secant stiffness at any displacement, S_{oi} = the secant stiffness at 1mm, x_i = the abutment displacement, λ = a constant, and i takes L, V, and T for longitudinal, vertical,

and transverse stiffnesses respectively. Equation 1 is reproduced below in a nondimensional form as

$$S_i = D_i E_i \left(\frac{X_i}{H}\right)^{-G_i I_i} \tag{16}$$

in which S_i = the secant stiffness in kN/m/m width of wall, D_i and G_i are dimensionless factors, and E_i and I_i are the normalizing factors given by

$$E_L = E_V = \frac{\gamma B^3}{H^2} \tag{17a}$$

$$E_T = \frac{\gamma B W^2}{H^2} \tag{17b}$$

$$I_L = I_V = \frac{H k_h}{B}$$

and

$$I_T = \frac{H k_h}{W} \tag{18b}$$

Here, γ = the unit weight of the soil and W = the width of the abutment in the transverse direction. These relationships have been developed by closely inspecting the abutment deformation model described above. For example, the resistance for abutment rotation at low longitudinal displacements is proportional to B^3 while the abutment top displacement is proportional to H. These observations have been used to arrive at the appropriate normalizing factors, E_i and I_i.

For D_i, there are three plots for each of the translational spring (i.e. D_L, D_V, and D_T) and these are shown in Figs. 29a, 29b, and 29c. Figures 30a, 30b, and 30c give the G_i values. The D_i values for all stiffnesses show that D_i is proportional to abutment height but inversely

proportional to the excitation strength, k_h. Though G_i values exhibit a similar trend with respect to the excitation strength, the variation is inversely proportional to abutment height (see Figs. 30a, 30b, and 30c).

MODIFICATION TO DESIGN CURVES

The design curves provided above are for typical or "baseline" cases in which representative values for many parameters have been assumed. For example, the vertical deck-abutment interaction load, V_D = 250 kN/m, the abutment width in the transverse direction, W = 10m, and, also, the soil properties shown in Table 2 have been used in the development of the design curves. However, in the event that these values no longer apply, the stiffnesses given by the design curves need to be modified. An attempt to quantify these modification factors is presented below.

A single but representative medium high abutment (Wall 5 in Table 4) 4.5m high, designed for a seismic coefficient of k_h = 0.15 (a_{max} = 0.3g), was used to produce the stiffness plots with the "baseline" parameters and modified parameters. Figure 31 shows the predicted differences in all of the translational stiffnesses (S_L, S_V, and S_T) between the baseline case and the case with V_D changed to 500 kN/m. All of the other parameters have been kept the same. When V_D is changed, a new abutment (Wall A) has to be designed such that it has adequate factors of safety against static and dynamic loading (Table 2). It may be noted that the vertical stiffness given for V_D = 500 kN/m is lower, whereas other translational stiffnesses are higher when compared with the baseline case. By normalizing the stiffnesses given for V_D = 500 kN/m with respect to the baseline case, the modification factor R_{VD}, which accounts for the

influence of V_D, has been obtained and is presented in Fig. 32a. Similarly, two additional modification factors, R_W and R_ϕ, which account for the width, W, and the foundation soil failure angle, have also been developed using Wall A. In the case of R_W, the modified width is W = 20m and, for R_ϕ, the foundation soil friction angle is $\phi_f = 40°$. It may be noted that the baseline values used for W and ϕ_f are 10m and 35° respectively (see Table 3). Figures 32b and 32c give the modification factors, R_W and R_ϕ. Now, the stiffness given by Eq. 2 is modified as

$$(S_i)_{modified} = (S_i)_{Eq.\ 16} R_{VD} R_W R_\phi \qquad (19)$$

It is apparent from Fig. 32b that the vertical and longitudinal stiffnesses are not affected by the change in W. However, a substantial increase by a factor of as much as 1.7, irrespective of abutment displacement, is present in the case of translational stiffness. As expected, the vertical stiffness, S_V, has improved since the foundation soil friction angle has increased from 35° to 40°.

VERIFICATION OF DESIGN CURVES

The nine abutments used in the development of design curves cover abutment heights, H, from 3.5 to 6.5m and a horizontal excitation from a_{max} = 0.1g to 0.5g. To verify the validation of the applicability of the design curves, stiffnesses were computed using the approach for a 4.0m high abutment subjected to a horizontal base excitation with a_{max} = 0.4g; these were then compared with those given by the design curves. The height of the abutment and design excitation level were selected such that they did not represent a case used to developed the design curves. The abutment dimensions were obtained from the optimum

design procedure of Siddharthan et al. (1994). The wall dimensions are the same as those for Wall 4 shown in Table 4 except A_5 = 0.1m , A_6 = 1.2m, and B = 2.6m. Figure 33 shows the plots for the computed results and those predicted from design curves for all translational spring stiffnesses. An inspection of this figure suggests that the stiffnesses given by Eq. 16 are adequate to predict abutment stiffnesses.

CONCLUSIONS

This report presents an efficient approach, based on many well-established soil mechanics principles, to evaluate the nonlinear translational spring stiffnesses to represent seat-type abutments. The applicability of previous studies is limited because such studies are incapable of handling many important factors such as nonlinear soil behavior, free-field strains induced by an earthquake, the influence of wing walls, and the difference in soil behavior under active and passive conditions. The proposed approach accounts for all of these factors. The procedures adopted in this approach are relatively simple, and emphasis has been placed on easy interpretation and on achieving consistency between design procedures routinely used in the static and seismic design of abutments. For example, concepts such as the development of active and passive conditions in the soil surrounding the abutment and the failure of the foundation after reaching ultimate bearing capacity, the presence of inertia forces under seismic excitation, etc. have been incorporated into the analysis. The number of material parameters required for the model have been kept to a minimum. Only routinely used soil properties, such as the relative density, unit weight, angle of internal friction, and interface friction angles, are required in the model.

The equivalent linear elastic approach, which is widely used in seismic response studies, has been adopted to model the nonlinear stress-dependent behavior of soil. By defining the (1) nonlinear response of backfill soil to lateral movement and (2) resistance to translation and rotation at the abutment base, it is possible to construct a procedure to characterize nonlinear abutment stiffnesses.

A numerical example pointing out many of the intermediate steps employed in the approach have also been presented. The results reported for the medium high abutment show the influence of free-field strains from earthquake excitation on the abutment stiffnesses. The approach described herein provides a realistic procedure in which a number of important factors that govern abutment stiffness behavior have been accounted for. The approach presented to obtain abutment stiffnesses is considered much more efficient and appealing to practicing engineers than other comparable methods such as the finite element method.

The second part of the study presents (1) a validation study undertaken to verify the predictive capability of the proposed procedures, and (2) ready to use design curves to compute abutment stiffnesses. The verification study utilized data from a recently conducted large-scale field test. Both longitudinal and transverse field tests were carried out, and a displacement in the transverse test was as much as 180mm. The abutments were equipped with wing walls and supported poorly graded medium dense clean sand. An excellent agreement was observed between the proposed approach and the field test results. The failure surface developed behind the abutment and the displacement mechanism that were interpreted from excavation after the field test revealed that the assumptions made in the development of the proposed approach are valid.

Finally, the proposed approach has been used to develop ready to use design curves to estimate abutment stiffnesses. The design curves have been developed as a function of the height and width of the abutment and the seismic coefficient, k_h (Equation 16). Modification factors have also been developed to account for changes in the baseline parameters used in the development of the design curves (Equation 19). The applicability of the design curves has also been verified using an abutment that was not used in the development of the design curves.

ACKNOWLEDGEMENTS

This study was sponsored by the National Science Foundation Grant No. BCS-9221314 and a grant from the Nevada Department of Transportation. The support of these agencies is gratefully acknowledged.

REFERENCES

AASHTO guide specifications for seismic design of highway bridges. (1992). AASHTO.

Barker, R.M., Duncan, J.M., Rojiani, K.B., Ooi, P.S.K., Tan, C.K., and Kim, S.G. (1991). "Manuals for the design of bridge foundations." *NCHRP Rep. 343*, Transportation Research Board, Washington, D.C.

Buckle, I.G., Mayes, R.L., and Button, M.R., "Seismic design and retrofit manual for highway bridges," Report No. FHWA IP-87-6, FHWA, Washington, D.C.

Byrne, P.M., Cheung, H., and Yan, L. (1987). "Soil parameters for deformation analysis of soil masses." *Can. Geotech. J.*, Vol. 24, 366-376.

Chin, B.H. and Aki, K. (1991). "Simultaneous study of source, path and site effects on strong and weak motions," *Bull. Seism. Soc. Am.*, 81, 1,859-1,884.

Clough, G.W. and Duncan, J.M. (1991). *Foundation engrg. handbook*, 2nd Edition, Edited by H.Y. Fang, Van Nostrand Reinholdt, New York, NY, 223-235.

Crouse, C.B., Hushmand, B., Liang, G. Martin, G.R., and Wood, J. (1985). "Dynamic response of bridge-abutment-backfill systems," *Proc. joint U.S.-New Zealand workshop on seismic resistance of highway bridges*, San Diego, CA.

Crouse, C.B., Hushmand, B., and Martin, G.R. (1987). "Dynamic soil-structure interaction of a single-span bridge," *Earthquake Engrg. and Soil Dynamics*, 15, 711-729.

Douglas, B.M. and Saiidi, M. (1984). "Effect of design seismic loads on a highway bridge," *J. Struct. Engrg.*, ASCE, 110(11), 2,723-2,737.

Eberhard, M., Marsh, M.L., MacLardy, J., and Hjartarson, G. (1993). "Lateral load tests of a reinforced concrete bridge," Report to Washington State Dept. of Transp., Olympia, WA, by University of Washington, Dept. of Civil Eng., WA, August.

Engineering Manual. (1990). Settlement Analysis, EM1110-1-1904, U.S. Army Corps of Engineers, Washington, D.C.

Finn, W.D.L. (1988). "Dynamic analysis in geotechnical engineering," State-of-the-art Report, *Earthq. Engrg. and Soil Dyn. II*, Geotechnical Special Publication No. 20, Edited by L.V. Thun, ASCE, 523-592.

Gantes, C.J., Kanellaidis, G., and Kallivokas, D. (1989). "Impact of earthquakes on cantilever retaining walls." *J. of Struct. Engrg.*, ASCE, 115(10), 2,566-2,578.

Idriss, I.M. and Sun, J.I. (1992). "SHAKE91 - A computer program for conducting equivalent linear seismic response analyses of horizontally layered soil deposits," Dept. of Civil Engrg., Univ. of Calif., Davis, CA.

Lam, P.L. and Martin, G.R., "Seismic design of highway bridge foundations," FHWA Report No. FHWA/RD-86/101, 1986.

Lam, P.L., Martin, G.R., and Imbsen, R. (1991). "Modeling bridge foundations for seismic design and retrofitting," *Transportation Research Record*, No. 1290, 113-126.

Lee, K.W. and Finn, W.D.L. (1991). "DESRA-2C: Dynamic effective stress response analysis of soil," Dept. of Civil Engrg., Univ. of British Columbia, Canada.

Maragakis, E.A. and Jennings, P.C. (1987). "Analytical models for the rigid body motions of skew bridges." *J. of Earth. Engrg. and Struct. Dyn.*, 15, 923-944.

Maragakis, E.A. and Siddharthan, R. (1989). "A simple model for estimation of the nonlinear abutment stiffness in the longitudinal direction," *J. Struct. Engrg.*, ASCE, 115(9), 2,382-2,398.

Maragakis, E.A., Douglas, B.M., Vrontinos, S., and Abdel-Ghaffar, S. (1992). "Soil-structure interaction effects on the response of Meloland Bridge," *Proc. ASCE Structures Congress*, San Antonio, TX.

Maroney, B., Kutter, B., Romstad, K., Chai, Y.H., and Vanderbilt, E. (1994). "Interpretation of large scale bridge abutment test results," *Proc., 3rd Annual Seism. Research Workshop*, CalTrans, Sacramento, CA.

McCallen, D.B. and Romstad, K.M. (1994). "Dynamic analyses of a skewed, short-span, box girder overpass," *Earthquake Spectra*, 10(4), 729-756.

NAVFAC DM 7.2. (1982). *Foundations and earth retaining structures design manual*, Dept. of the Navy, Alexandria, VA.

Poulos, H.G. and Davis, E.H. (1974). *Elastic solutions for soil and rock mechanics*, John Wiley and Sons Inc., New York, NY.

Richards, R., Elms, D.G., and Budhu, M. (1993). "Seismic bearing capacity and settlements of foundations," *J. Geotech. Engrg.*, ASCE, 119(4), 662-674.

Schmertmann, J.H. (1970). "Static cone to compute static settlement over sand," *J. Soil Mech. and Found. Div.*, ASCE, 96(3), 1,011-1,043.

Schmertmann, J.H., Hartman, J.P., Brown, P.R. (1978). "Improved strain influence factor diagrams," Technical Notes, *J. Geotech. Engrg.*, ASCE, 104(8), 1,131-1,135.

Schnabel, P.B., Lysmer, J., and Seed, H.B. (1972). "SHAKE: A computer program for earthquake response analysis of horizontally layered sites," *Report No. EERC 72-12*, College of Engrg., Univ. of calif., Berkeley, CA.

Seed, H.B. and Idriss, I.M. (1970). "Soil moduli and damping in soils, design equation and curves." *Rep. No. EERC 70-10*, Earthquake Engineering Research Center, University of California, Berkeley.

Seed, H.B. and Whitman, R.V. (1970). "Design of earth retaining structures for dynamic loads," *Specialty Conf. on Lateral stresses in the Ground and Design of Earth Retaining Struct.*, ASCE, New York, 103-147.

Seed, H.B. (1983). "Earthquake-resistant design of earth dams," *Proc., Seismic Design of Embankments and Caverns*, ASCE, 41-64.

"Seismic design of reinforced earth retaining walls and bridge abutments - practical design method." (1990). Reinforced Earth Company, McLean, VA.

Siddharthan, R., Ara, S., and Norris, G.M. (1992). "Simple rigid plastic model for seismic tilting of rigid walls," *J. Struct. Engrg.*, ASCE, 118(2), 469-487.

Siddharthan, R., El-Gamal, M., and Maragakis, E.A. (1994). "Investigation of performance of bridge seismic regions," *J. Struct. Engrg.*, ASCE, 120(4), 1,327-1,346.

Siddharthan, R., El-Gamal, M., and Maragakis, E.A. (1995). "Nonlinear bridge abutment stiffnesses: verification and design curves," Submitted for publication in *J. Struct. Engrg.*, ASCE.

Tsai, N.C., Firouz, A., Sedart, H., and Werner, S.D. (1993). "Applications of Caltrans' current seismic evaluation procedures for selected short bridge overcrossing structures," Report submitted to Caltrans, Contract No. 59Q122, Dames and Moore, Oakland, CA.

Tokimatsu, K. and Seed, H.B. (1987). "Evaluation of settlement in sands due to earthquake shaking," *J. Geotech. Engrg.*, ASCE, 113(8), 861-878.

Ueng, J., Hutchins, L., Jarpe, S., Kasameyer, P., and Heuze, F. (1994). "A new, combined seismic-geotechnical approach for estimating site-specific strong motion: application to the Painter Street Bridge site, Rio Dell, California," 3rd Annual Seism. Research Workshop, CalTrans, Sacramento, CA.

Werner, S.D., Beck, J.L., and Levine, M.B. (1987). "Seismic refraction evaluation of Meloland Road Overpass using the 1979 Imperial Valley earthquake records," *Earthquake Engrg. and Struct. Dyn.*, 15, 249-274.

Werner, S.D., Beck, J.L., and Nisar, A. (1990). "Dynamic tests and seismic excitation of a bridge structure," *Proc., 4th National Conf. on Earthquake Engrg.*, EERI, Palm Springs, CA, 1, 1,037-1,046.

Werner, S.D. (1994). "Study of Caltrans' seismic evaluation procedures for short bridges," *Proc., 3rd Annual Seism. Research Workshop*, CalTrans, Sacramento, CA.

Whitman, R.V. (1990). "Seismic design and behavior of gravity retaining walls," *Des. and Perf. of Earth Retaining Struct.*, Geotech. Special Publication, No. 25, ASCE, New York, NY, 817-842.

Whitman, R.V. (1991). "Seismic design of earth retaining structures (state-of-the-art paper)," *Proc., 2nd Int. Conf. on Recent Adv. in Geotech. Earthquake Engrg. and Soil Dynamics*, St. Louis, MO, II, 1,767-1,778.

Wilson, J.C. (1988). "Stiffness of non-skew monolithic bridge abutments for seismic analysis," *Earth. Engrg. and Struct. Dyn.*, 16, 867-883.

Wilson, J.C. and Tan, B.S. (1990). "Bridge abutments: formulation of simple model for earthquake response analysis," *J. Engrg. Mech.*, ASCE, 116(8), 1,828-1,837.

Yu, G., Anderson, J.G., and Siddharthan, R. (1993). "On the characteristics of nonlinear soil response," *Bull. Seism. Soc. Am.*, 83, 218-244.

TABLE 1: ABUTMENT DIMENSION AND SOIL PROPERTIES USED IN THE PARAMETRIC STUDY

PARAMETERS	VALUES
DIMENSIONS	
H (m)	4.5
H_p (m)	2.75
A_1, A_2, A_3 (m)	0.3, 1.0, 1.0
A_4, A_5, A_6 (m)	0.75, 0.1, 2.5
C_1, C_2, C_3 (m)	0.1,1.0,4.25
B (m)	3.9
W (2 Lanes) (m)	10.0
DECK FORCES	
V_D (kN/m)	500
H_D (kN/m)	200
SOIL PROPERTIES	
Angle of Internal friction of Backfill, ϕ_b	35^0
Backfill Interface Friction angle, δ_b	15^0
Foundation Soil Friction angle, ϕ_f	35^0
Foundation Soil-Base Interface Angle, δ_f	21^0
Unit weight of Soil, γ (kN/m^3)	18.5
Poisson's Ratio, υ	0.3
$(K_2)_{max}$	55
FACTORS OF SAFETY	
(STATIC)	
1) Sliding	2.23
2) Overturning	4.83
3) Bearing Capacity	10.33
(DYNAMIC)	
1) Sliding	1.13
2) Overturning	1.96
3) Bearing Capacity	1.51

Table 2: Soil Properties Used in Verification Study

Parameter	Value
Unit weight of soil, γ (kN/m^3)	18.5
Backfill friction angle, ϕ_b (°)	40
Backfill-abutment interface friction angle, δ_b (°)	15
Foundation soil friction angle, ϕ_f (°)	35
Foundation-base friction angle, δ_f (°)	21
Foundation soil , $(K_2)_{max}$	55
Poisson's ratio, ν	0.3

Table 3: Factors of Safety for Various Failure Modes

Failure Mode	Static	Dynamic (pseudostatic)
F.O.S. against sliding	1.5	1.1
F.O.S. against overturning	2.0	1.5
F.O.S. against bearing failure	2.0	1.5
Tension development	No tension	---

Table 3. Abutments Used in the Development of Design Curves

Abutment Size	Abutment Height								
	H = 2.5 m			H = 4.5 m			H = 6.5 m		
Seismic Coefficient	k_h = 0.05	k_h = 0.15	k_h = 0.25	k_h = 0.05	k_h = 0.15	k_h = 0.25	k_h = 0.05	k_h = 0.15	k_h = 0.25
Wall No.	Wall 1	Wall 2	Wall 3	Wall 4	Wall 5	Wall 6	Wall 7	Wall 8	Wall 9
A_1, A_2 (m)	0.25,1.00	0.25,1.00	0.25,1.00	0.30,1.0	0.30,1.00	0.30,1.00	0.30,1.0	0.30,1.00	0.30,1.00
A_3, A_4 (m)	0.75,0.50	0.75,0.50	0.75,0.50	1.0,0.6	1.0,0.60	1.0,0.60	1.0,0.75	1.00,0.75	1.00,0.75
A_5, A_6 (m)	0.05,0.45	0.10,0.80	0.10,1.50	0.10,0.45	0.10,1.00	0.40,1.90	0.10,0.60	0.40,1.40	0.60,2.40
C_1, C_2 (m)	0.05,1.0	0.1,1.0	0.1,1.0	0.1,1.0	0.1,1.0	0.4,1.0	0.1,1.75	0.4,1.75	0.6,1.75
C_3 (m)	1.75	1.75	1.75	4.25	4.25	4.25	4.25	4.25	4.25
B,W (m)	1.75,10.0	2.15,10.0	2.85,10.0	1.85,10.0	2.4,10.0	3.60,10.0	2.0,10.0	3.10,10.0	4.30,10.0
H_p (m)	1.5	1.5	1.5	2.6	2.6	2.6	3.25	3.25	3.25
Factors of Safety Against Failure Modes: Dynamic Loading									
Sliding	1.52	1.14	1.10	2.33	1.66	1.22	2.55	1.81	1.28
Overturning	1.89	2.23	2.65	1.84	1.53	1.81	1.57	1.52	1.55
Bearing Failure	2.13	1.54	1.59	2.70	3.97	1.52	2.00	2.85	1.66

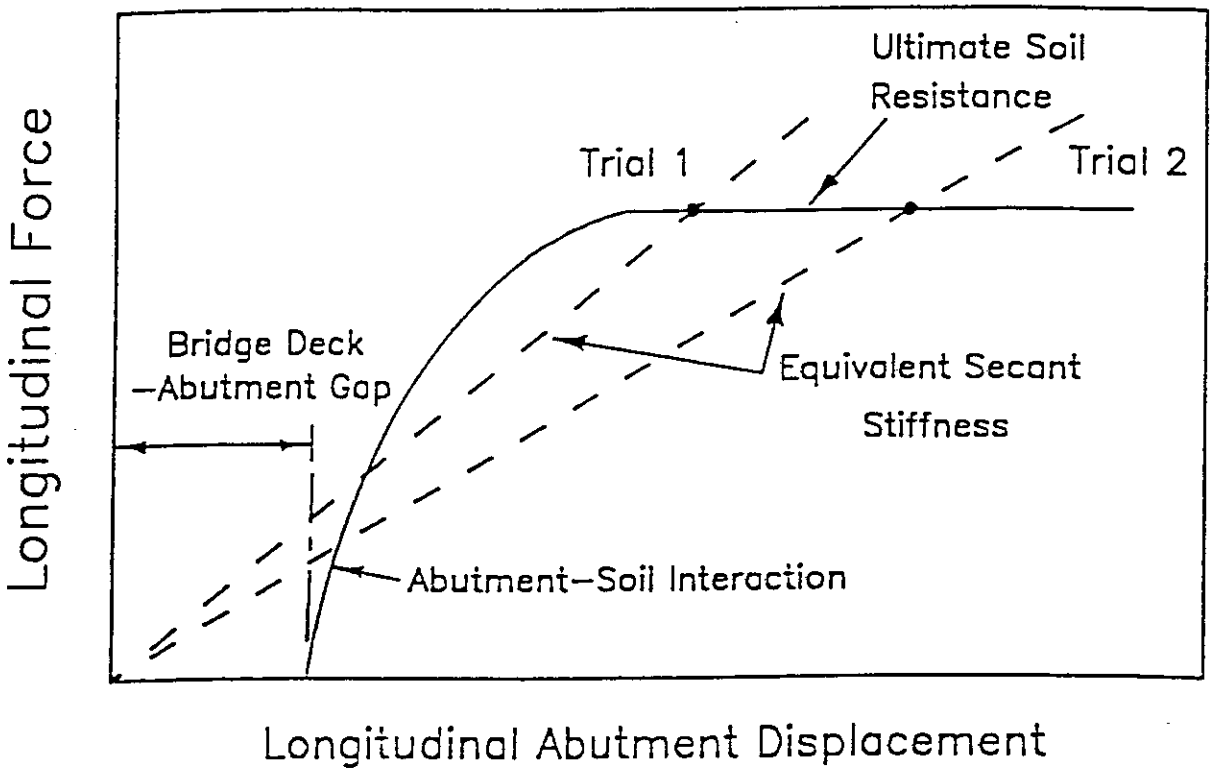

Fig. 1: Load-Displacement Characteristics of Seat-Type Abutments (After Lam et al., 1991).

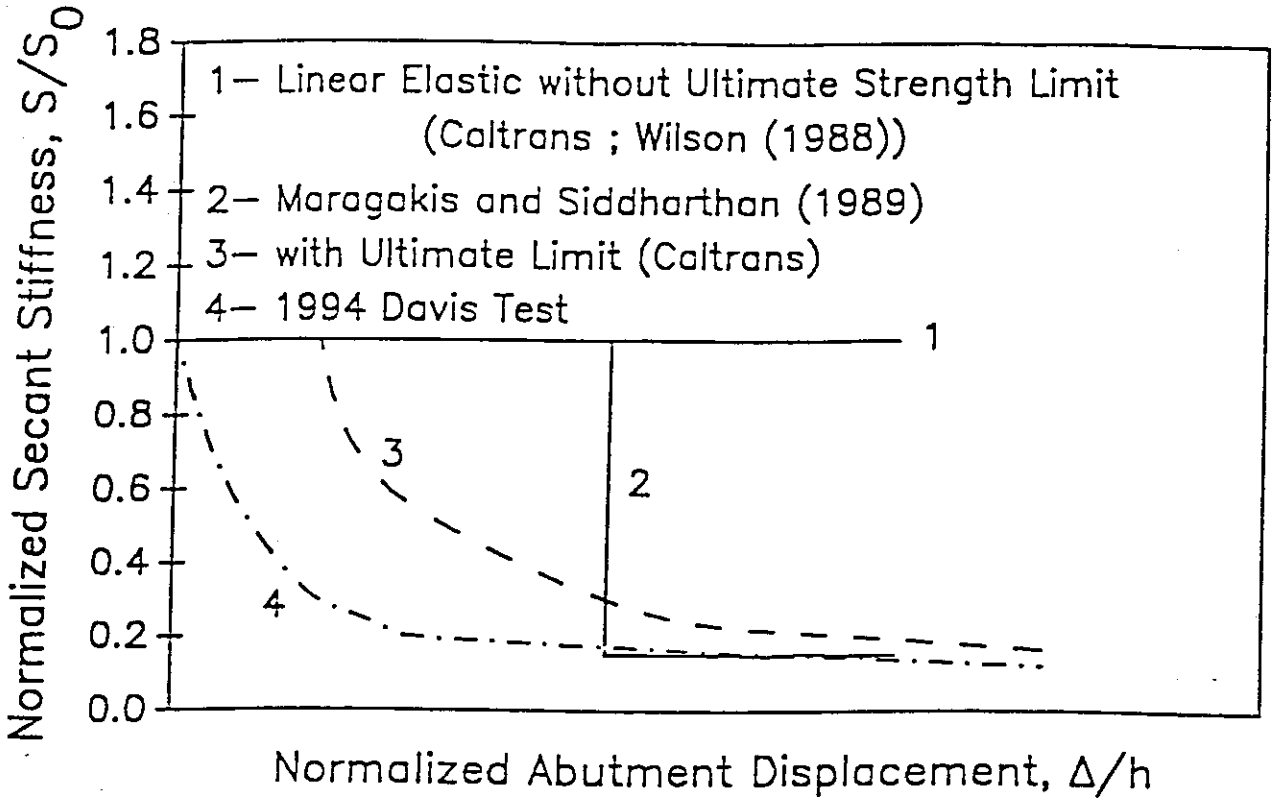

Fig. 2: Normalized Longitudinal Secant Abutment Stiffness from Past Studies.

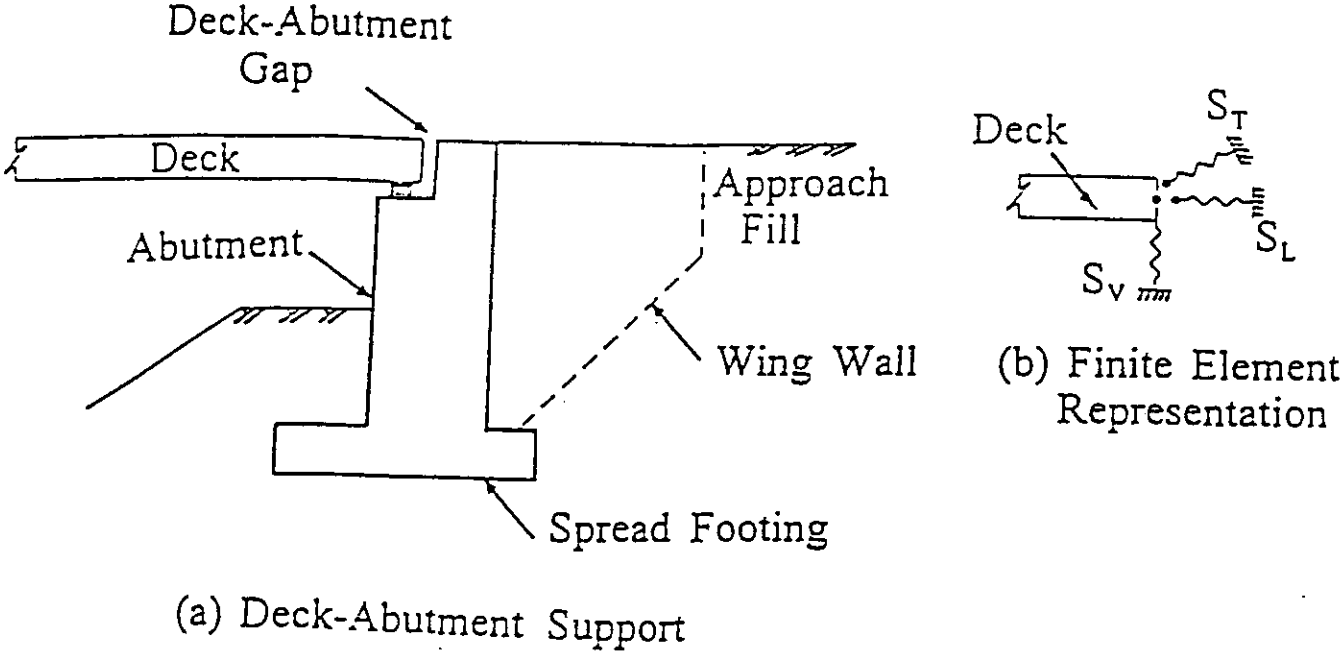

Fig. 3: Representation of Deck-Abutment-Backfill Interaction.

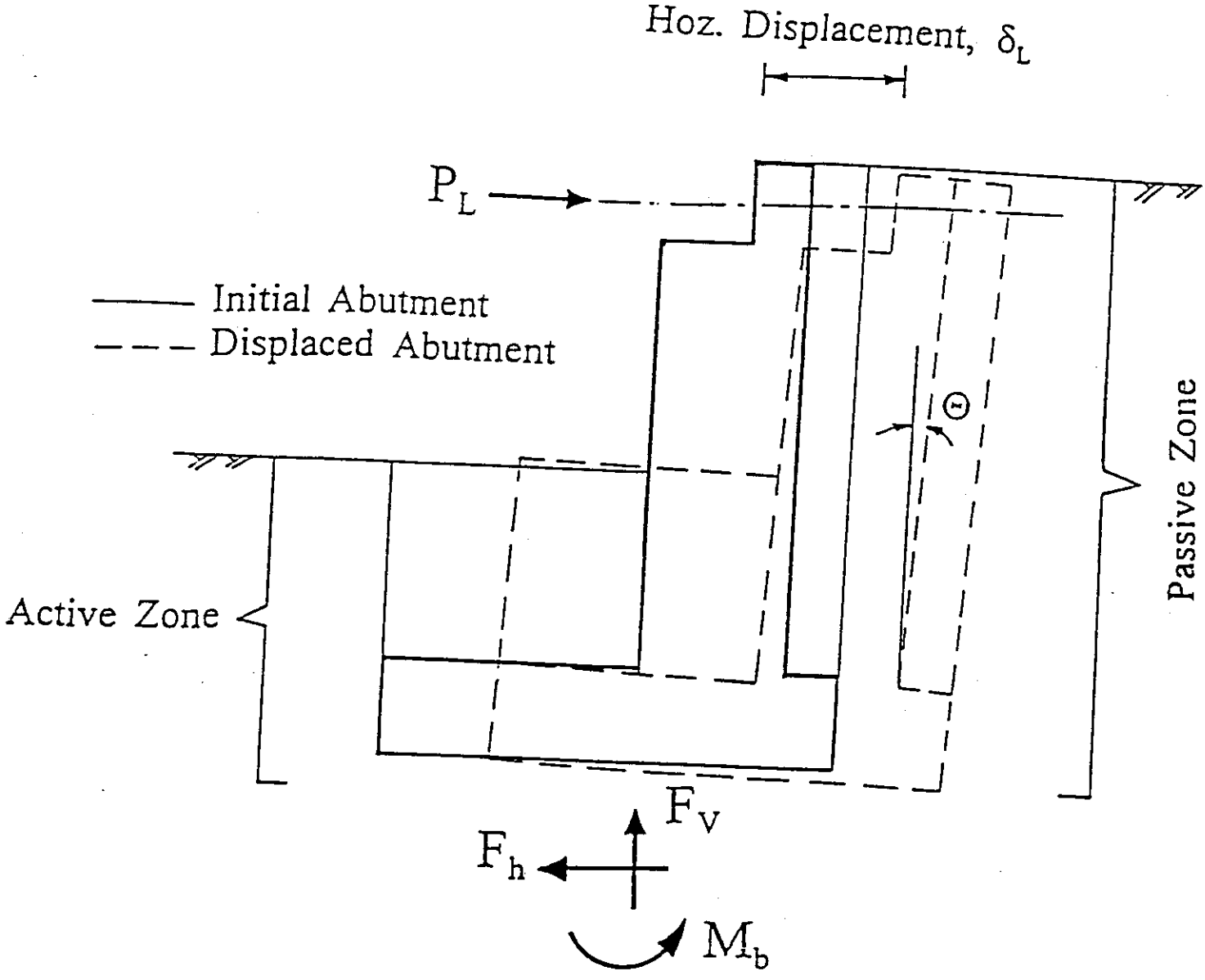

Fig. 4: Sketch of Displaced Abutment Caused by a Longitudinal Force.

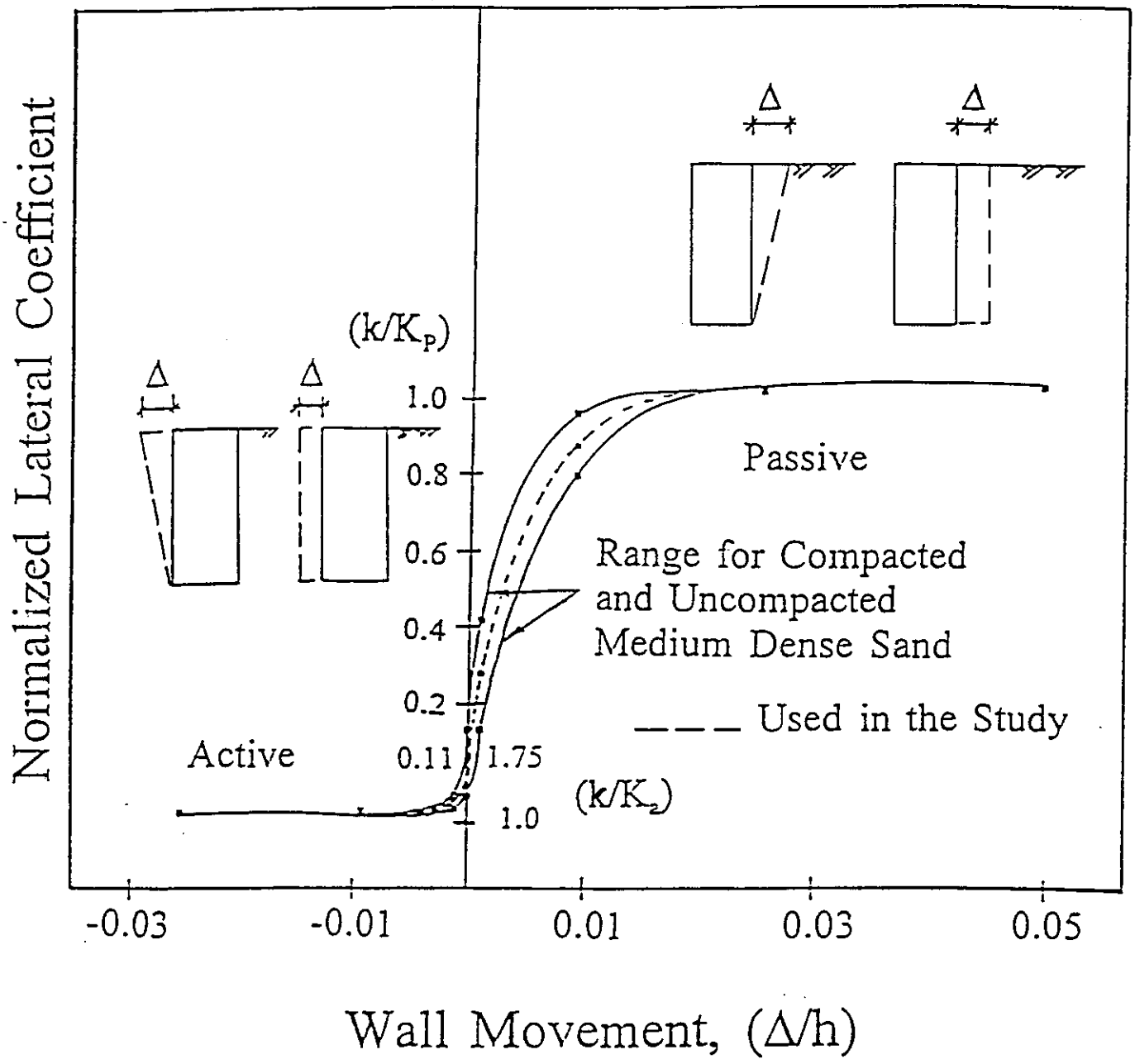

Fig. 5: Normalized Lateral Wall Pressure-Displacement Relationship (After Clough and Duncan, 1991).

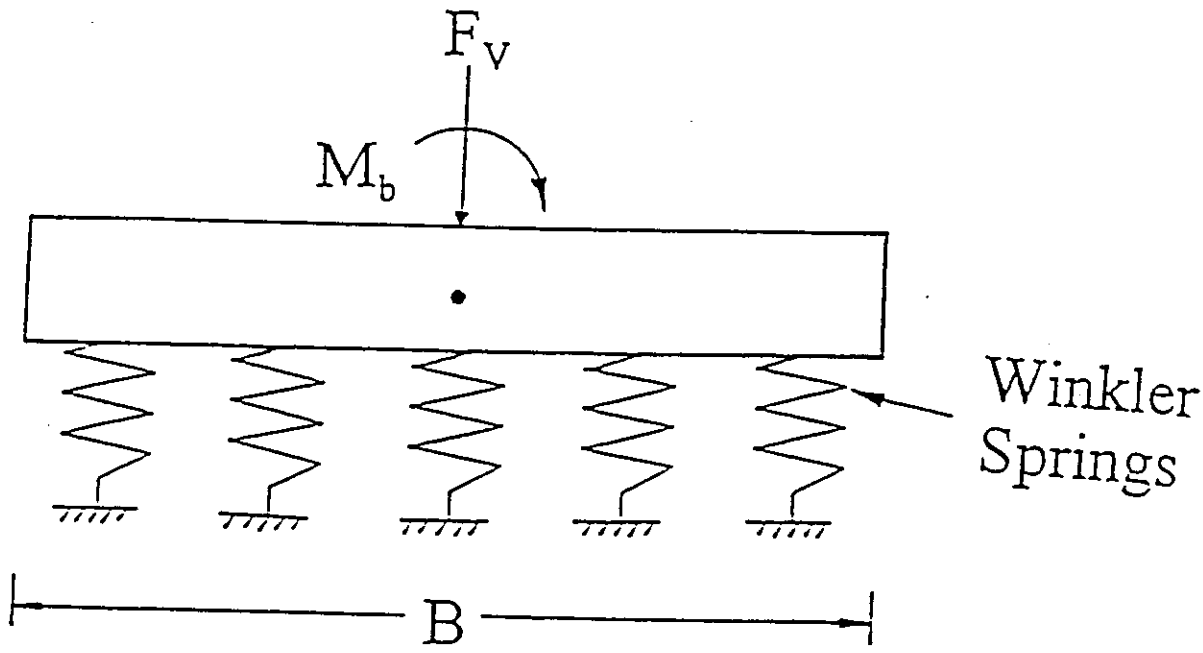

Fig. 6: Winkler Spring Representation for Abutment Base.

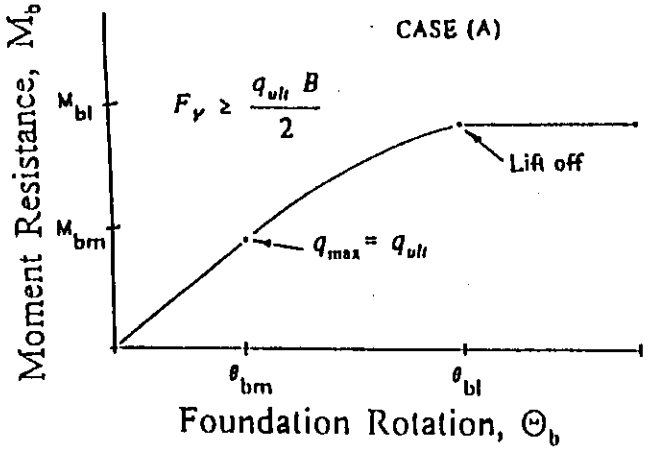

$$\theta \leq \theta_b \leq \theta_{cm} \qquad M_b = \frac{k_V\, B^3}{12}\, \theta_b$$

$$\theta_{cm} < \theta_b \leq \theta_{cl} \qquad M_b = 3M_{cm} - \sqrt{\frac{48\, M^3_{cm}}{k_V\, B^3\, \theta_b}}$$

$$\theta \geq \theta_{cl} \qquad M_b = 3M_{cm} - \frac{24\, M^2_{cm}}{q_{ult}\, B^2}$$

where

$$\theta_{cm} = \frac{12\, M_{cm}}{k_V\, B^3} \qquad \theta_{cl} = \frac{q^2_{ult}\, B}{12\, k_V\, M_{cm}}$$

and $$M_{cm} = (q_{ult} - \frac{F_V}{B})\, \frac{B^2}{6}$$

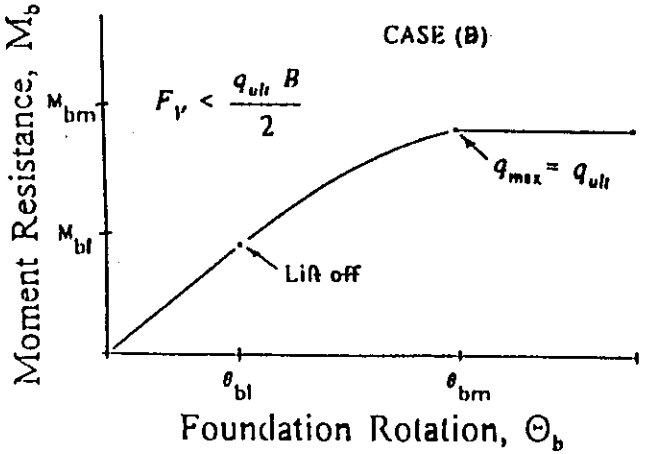

$$\theta \leq \theta_b \leq \theta_{bl} \qquad M_b = \frac{k_V\, B^3}{12}\, \theta_b$$

$$\theta_{bl} \leq \theta_b \leq \theta_{cm} \qquad M_b = F_V \left[\frac{B}{2} - \sqrt{\frac{2\, F_V}{9\, k_V\, \theta_b}} \right]$$

$$\theta \geq \theta_{cm} \qquad M_b = \frac{F_V}{6} \left[3B - \frac{4\, F_V}{q_{ult}} \right]$$

where

$$\theta_{cl} = \frac{2\, F_V}{k_V\, B^2} \qquad \text{and} \qquad \theta_{cm} = \frac{q^2_{ult}}{2\, F_V\, k_V}$$

Fig. 7: Moment-Rotation Relationship at the Base: Case A and Case B.

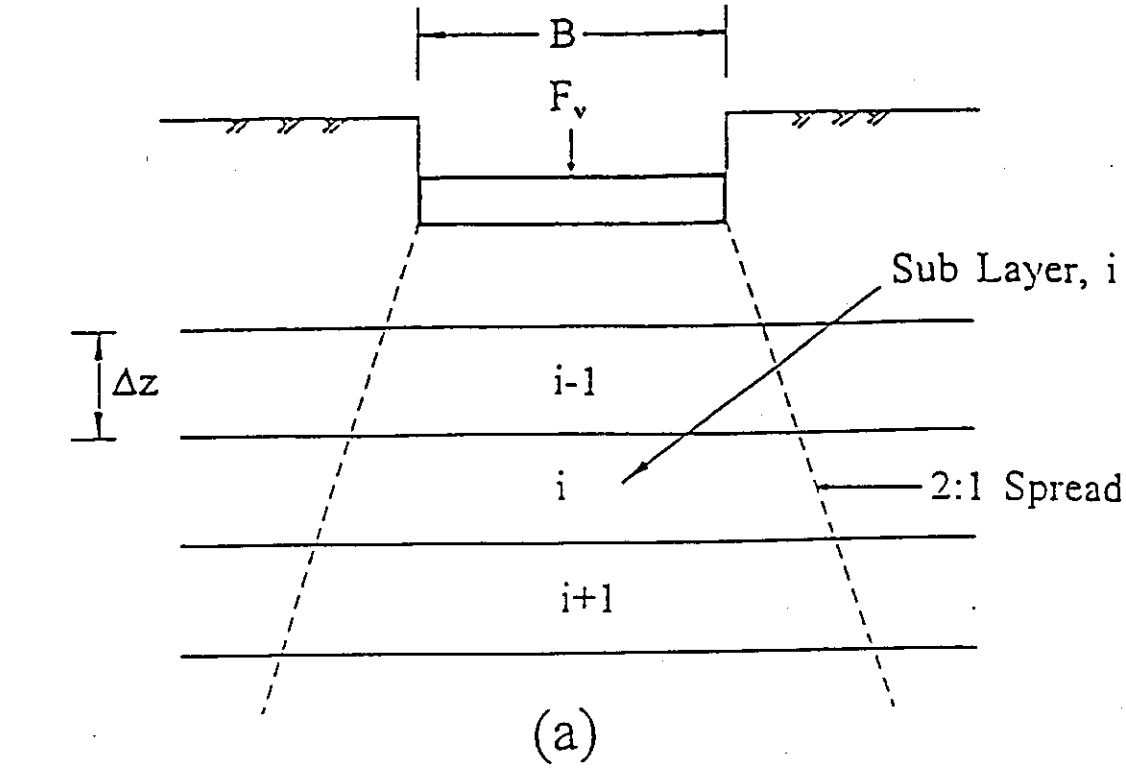

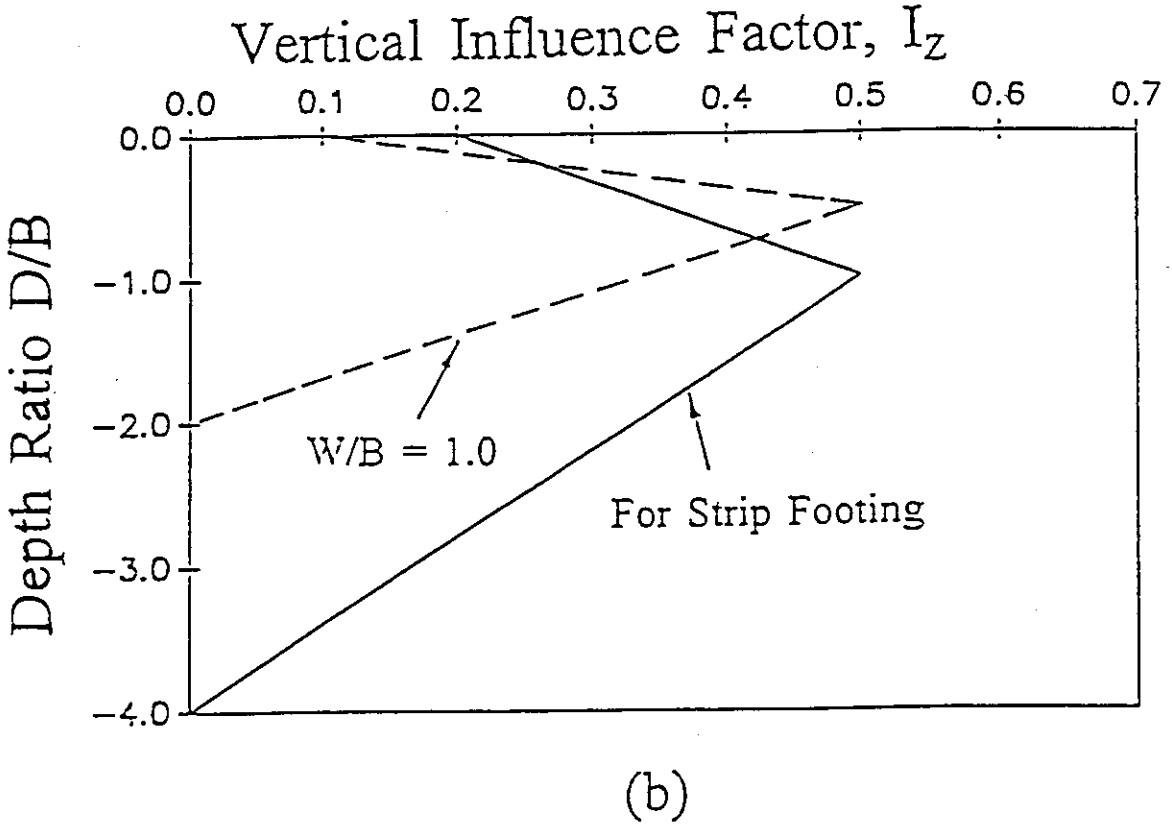

Fig. 8: Settlement Computation in sand from Schmertmann Procedure (a) Sublayers (b) Influence Factor, I_z.

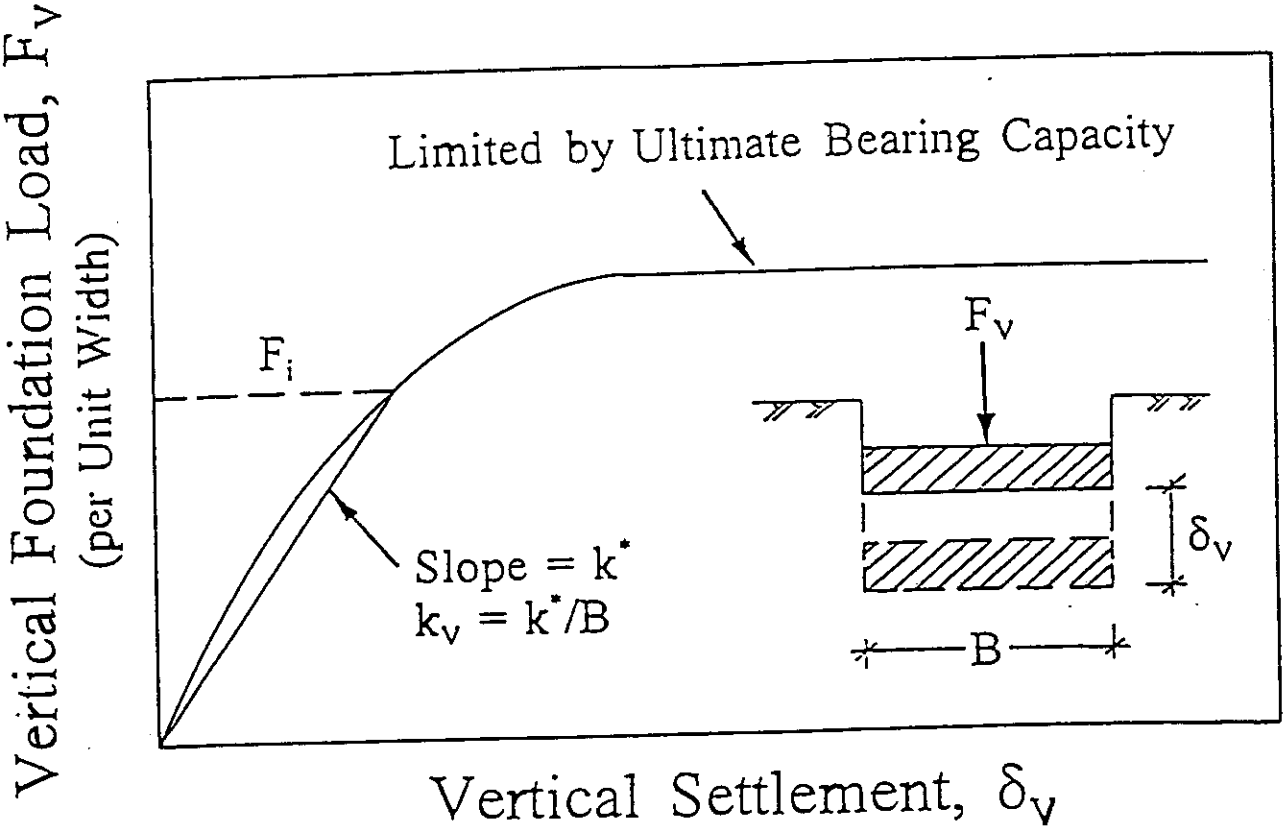

Fig. 9: Typical Nonlinear F_V-δ_V Relationship.

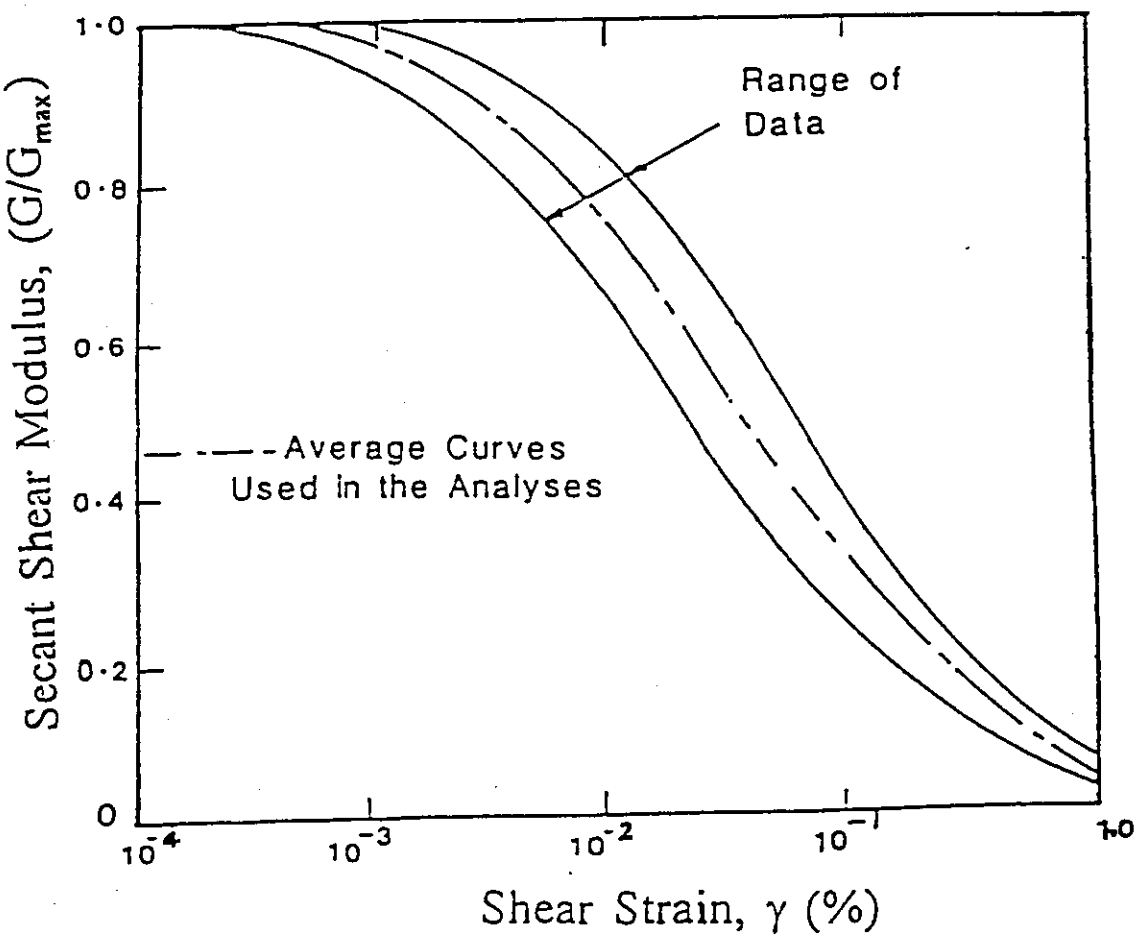

Fig. 10: Nonlinear Behavior of Sandy Soils (After Seed and Idriss, 1970).

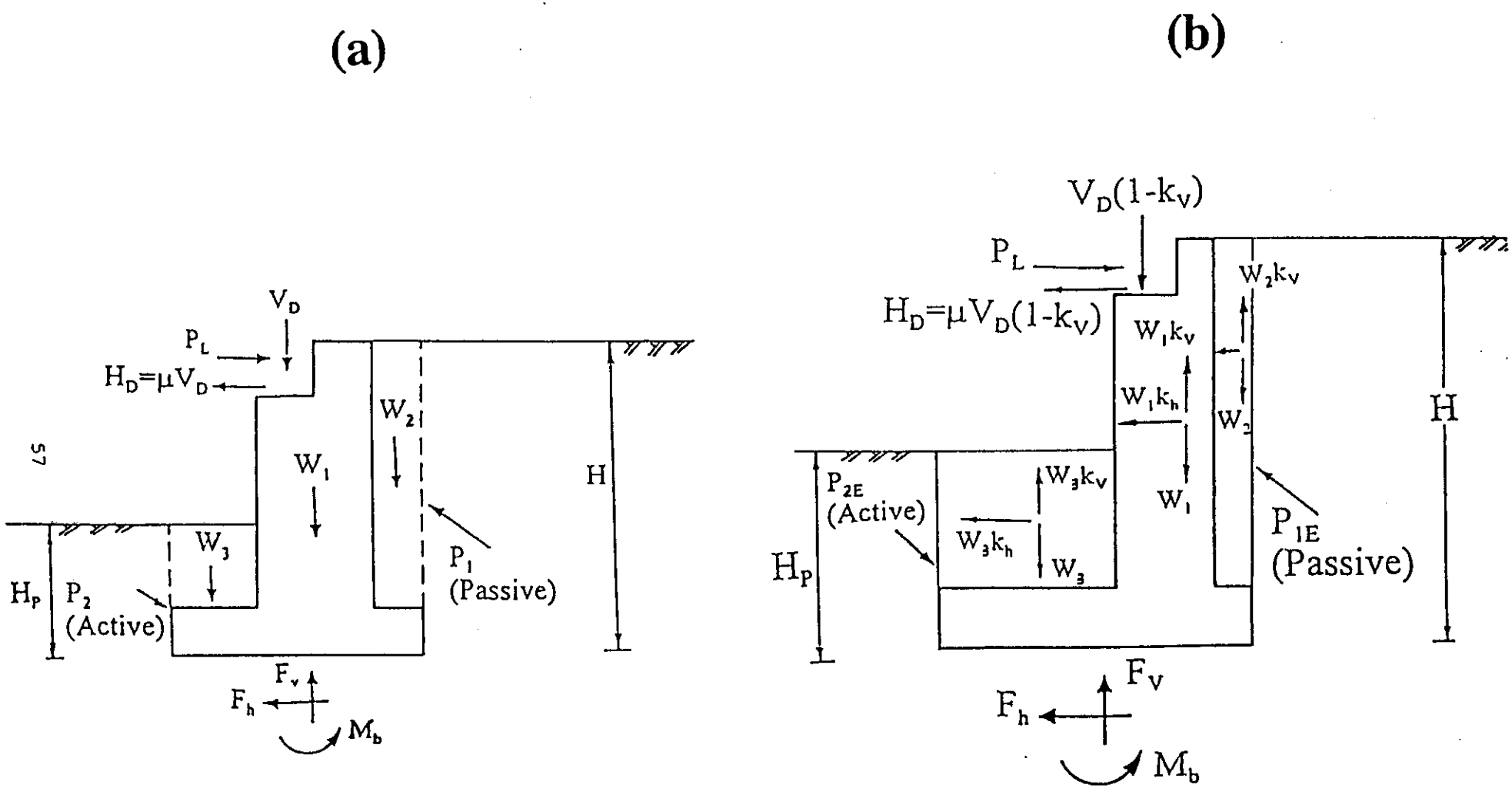

Fig. 11: Boundary Forces and Moments on the Abutment (a) Static Case (b) Pseudostatic Case.

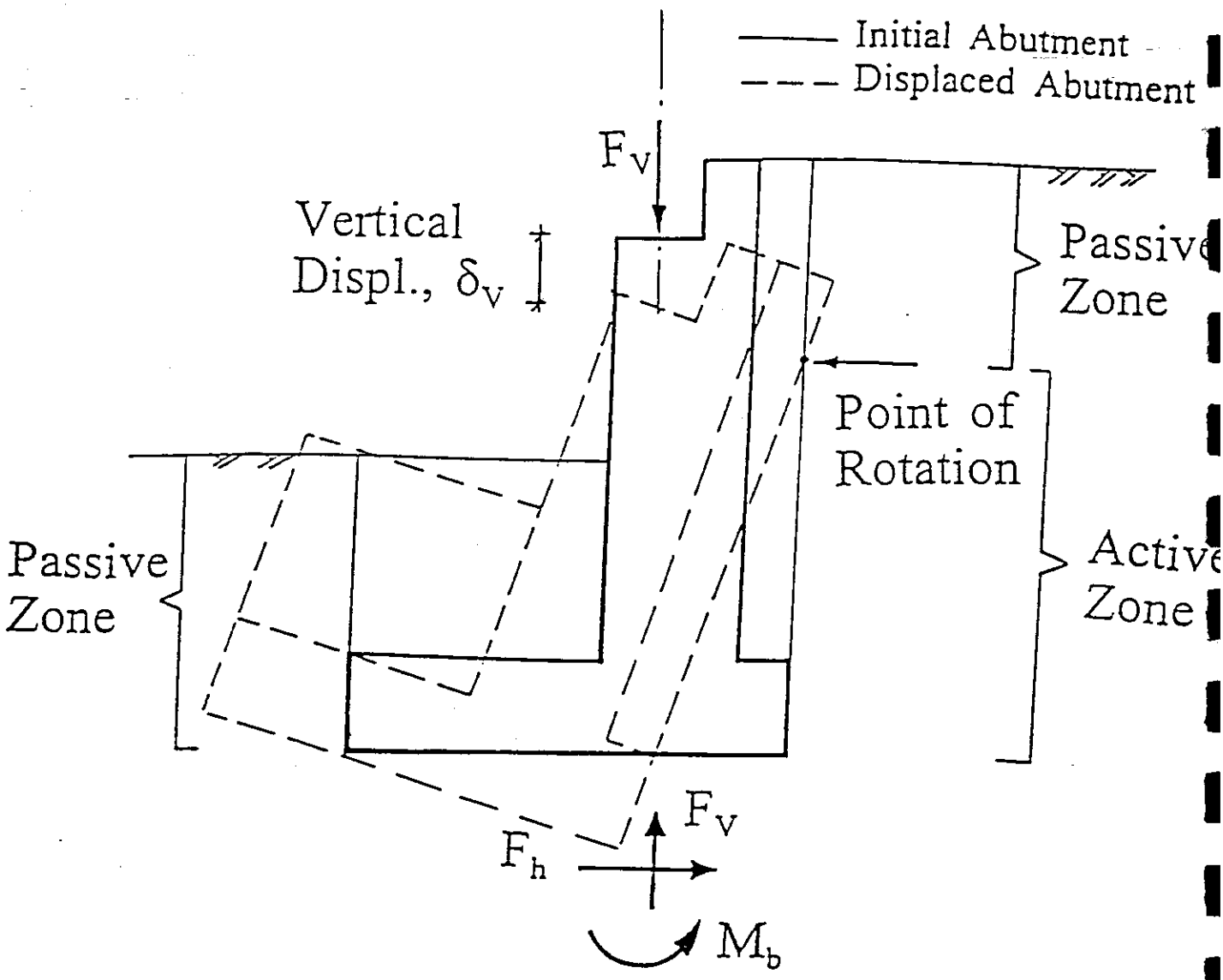

Fig. 12: Sketch of Abutment Movement for Vertical Stiffness Evaluation.

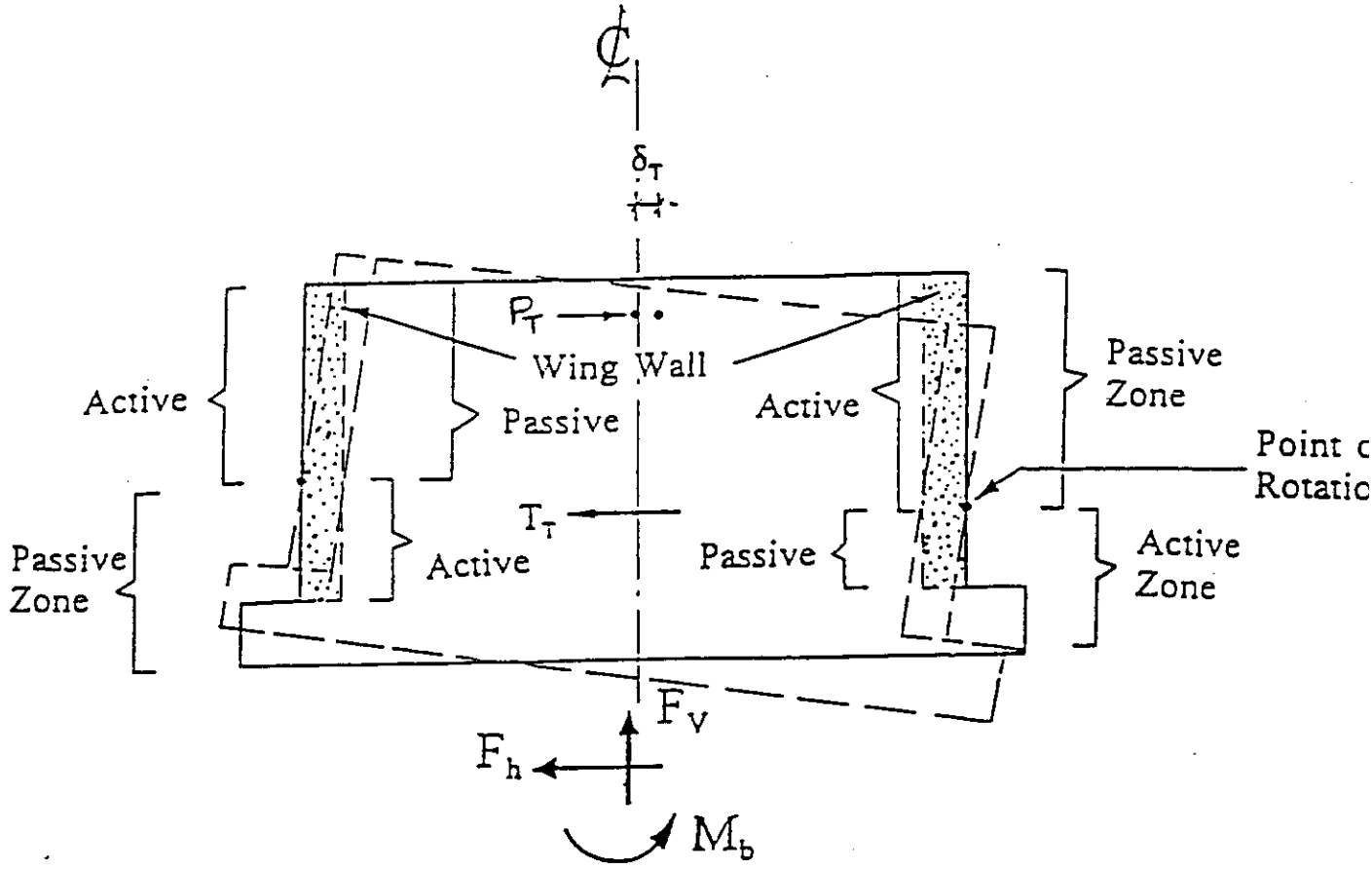

Fig. 13: Sketch of Abutment Movement for Transverse Stiffness Evaluation.

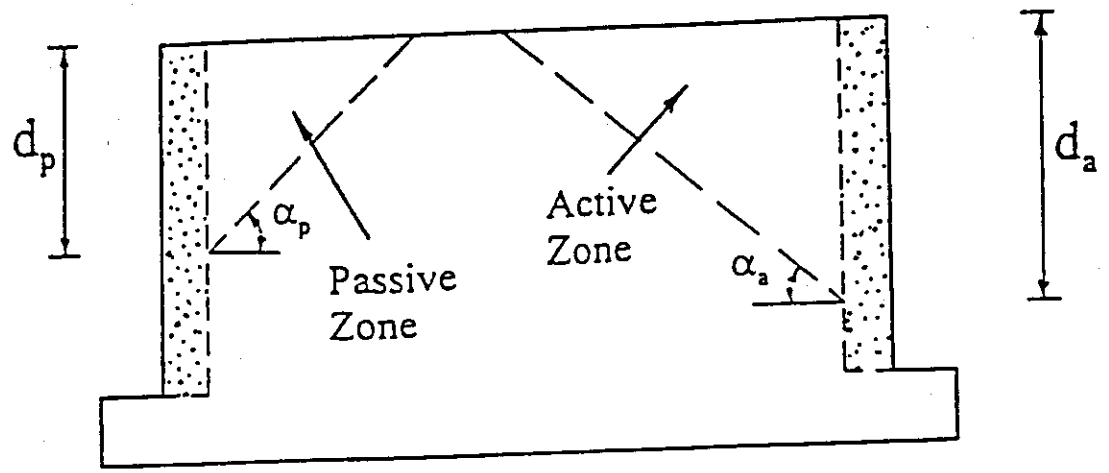

(a) No Overlap Between Failure Zones

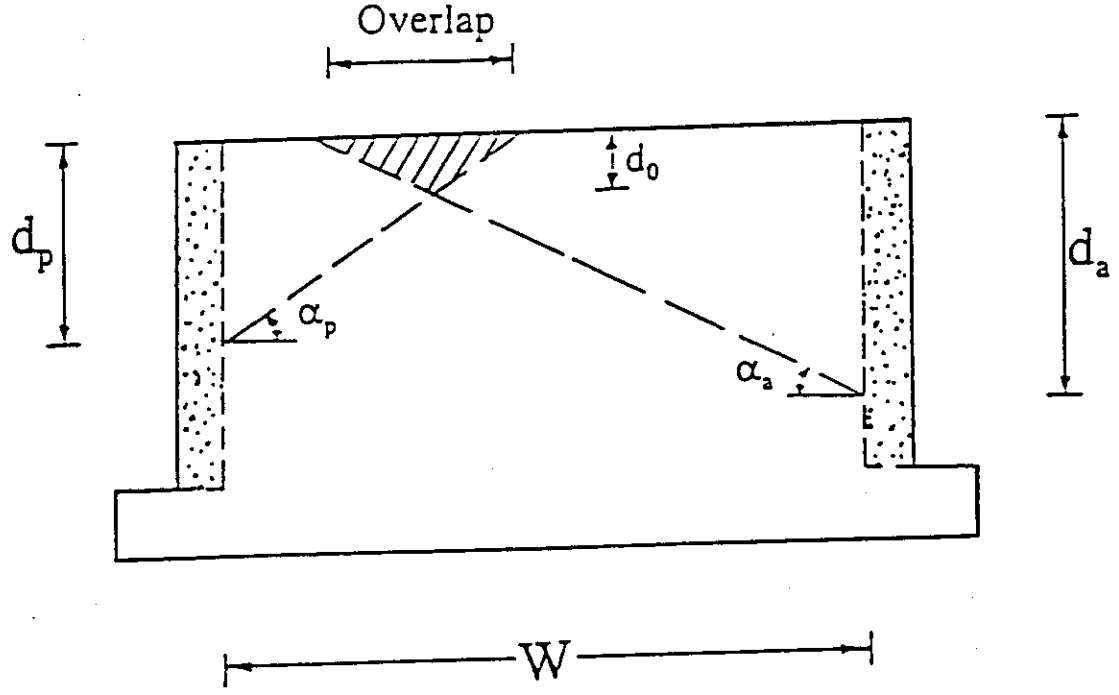

(b) Overlapping Failure Zones

Fig. 14: Modification for Earth Pressure due to Overlapping Failure Zones.

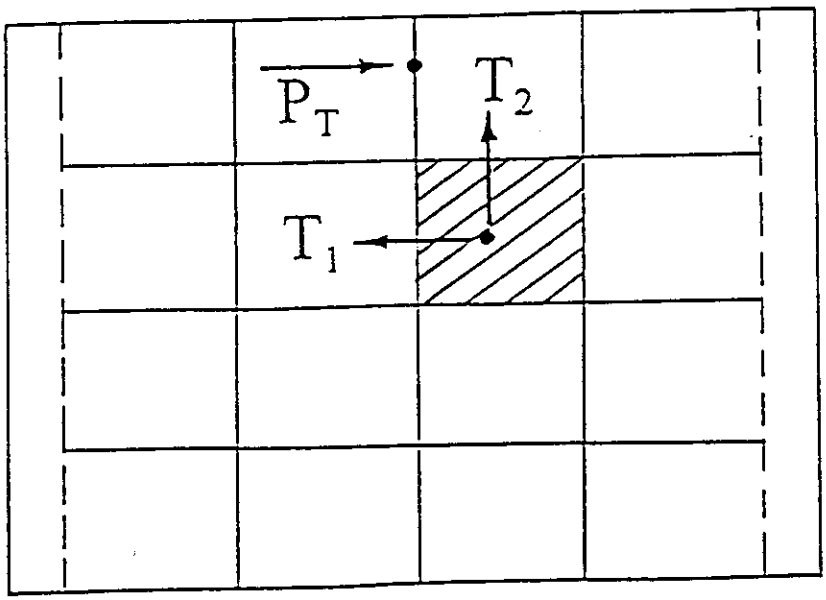

Fig. 15: Sub-Division of Abutment-Backfill Interface.

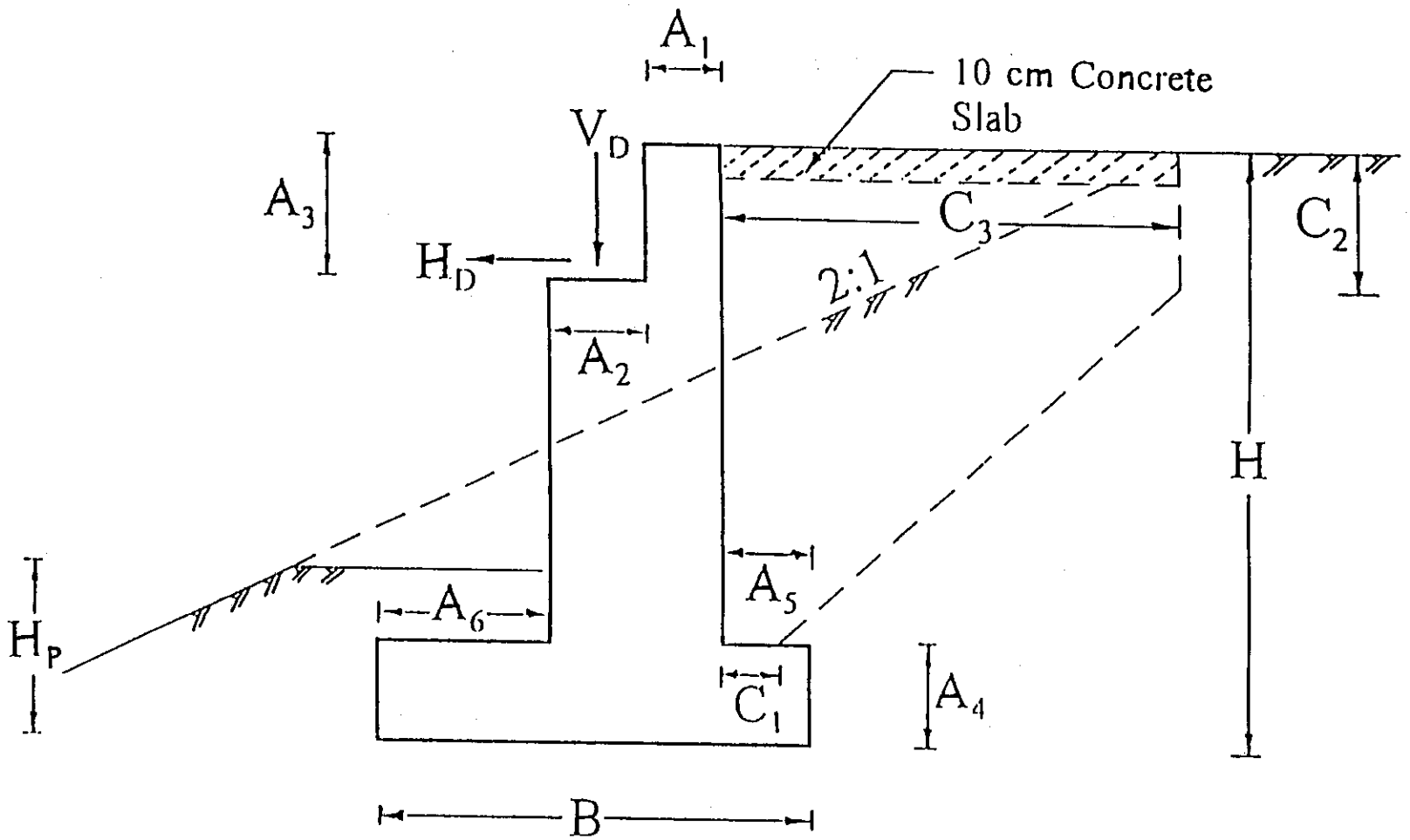

Fig. 16: Abutment Dimensions.

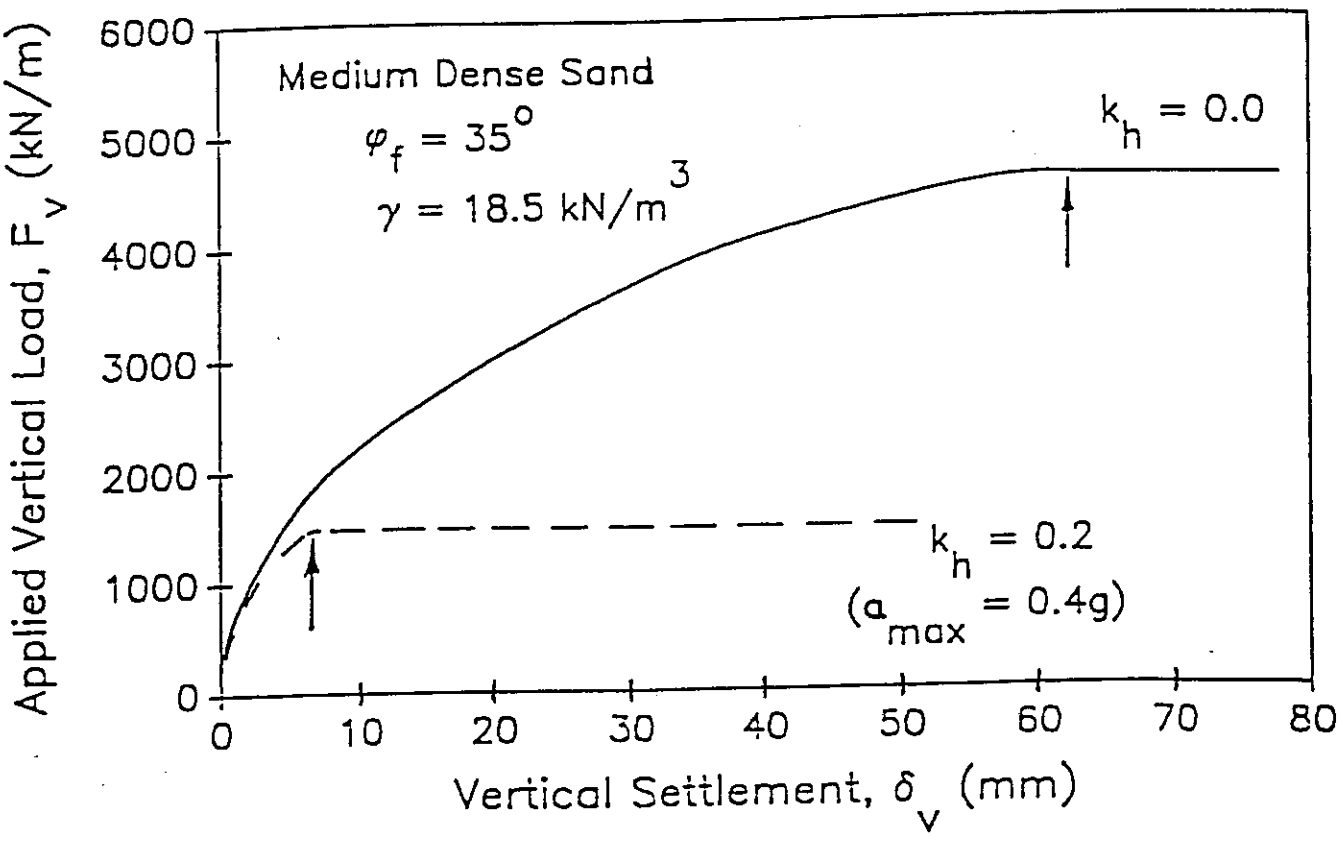

Fig. 17: F_v-δ_v Relationship at the Abutment Base.

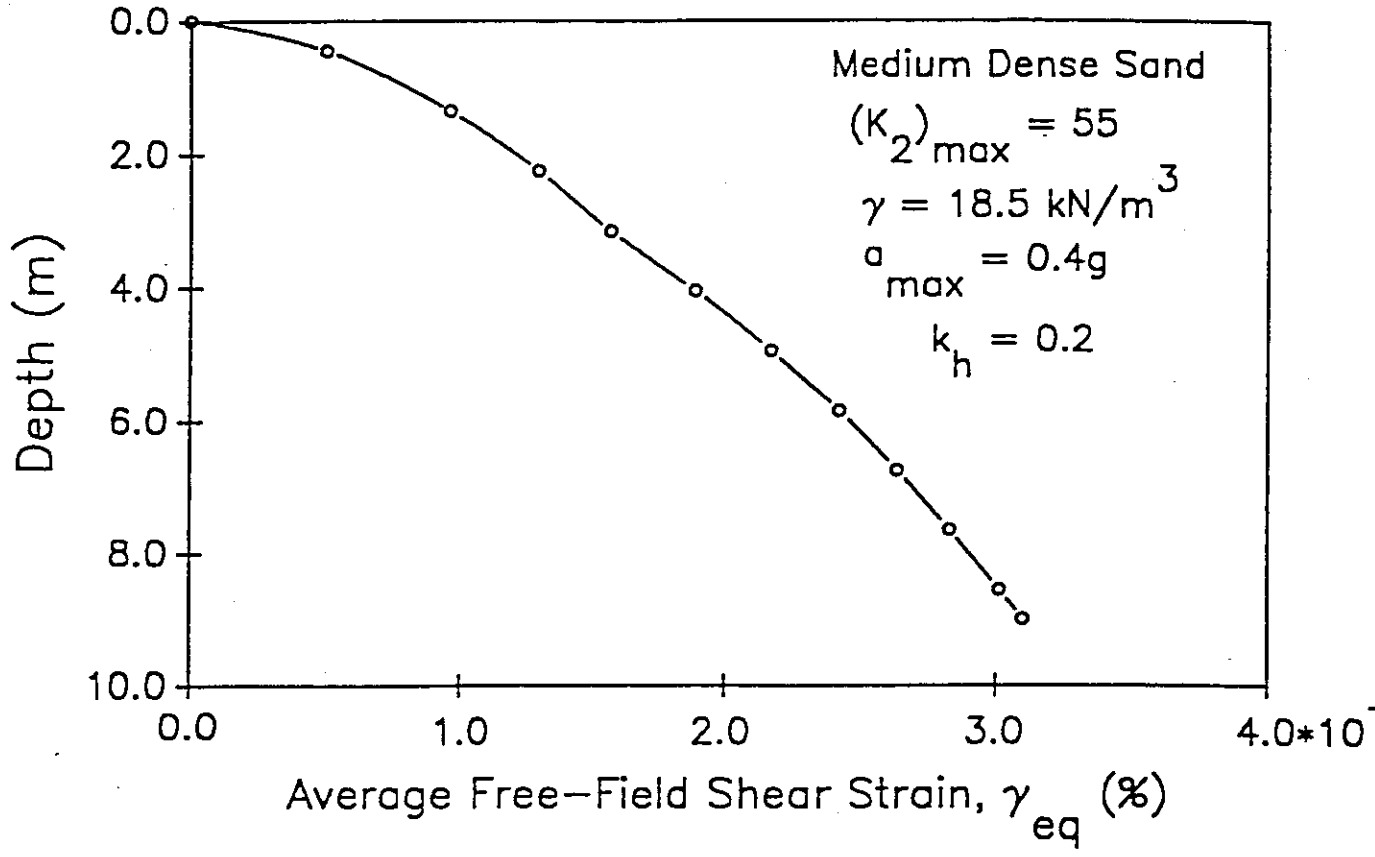

Fig. 18: Free-Field Shear Strains from Tokimatsu and Seed (1987) Procedure.

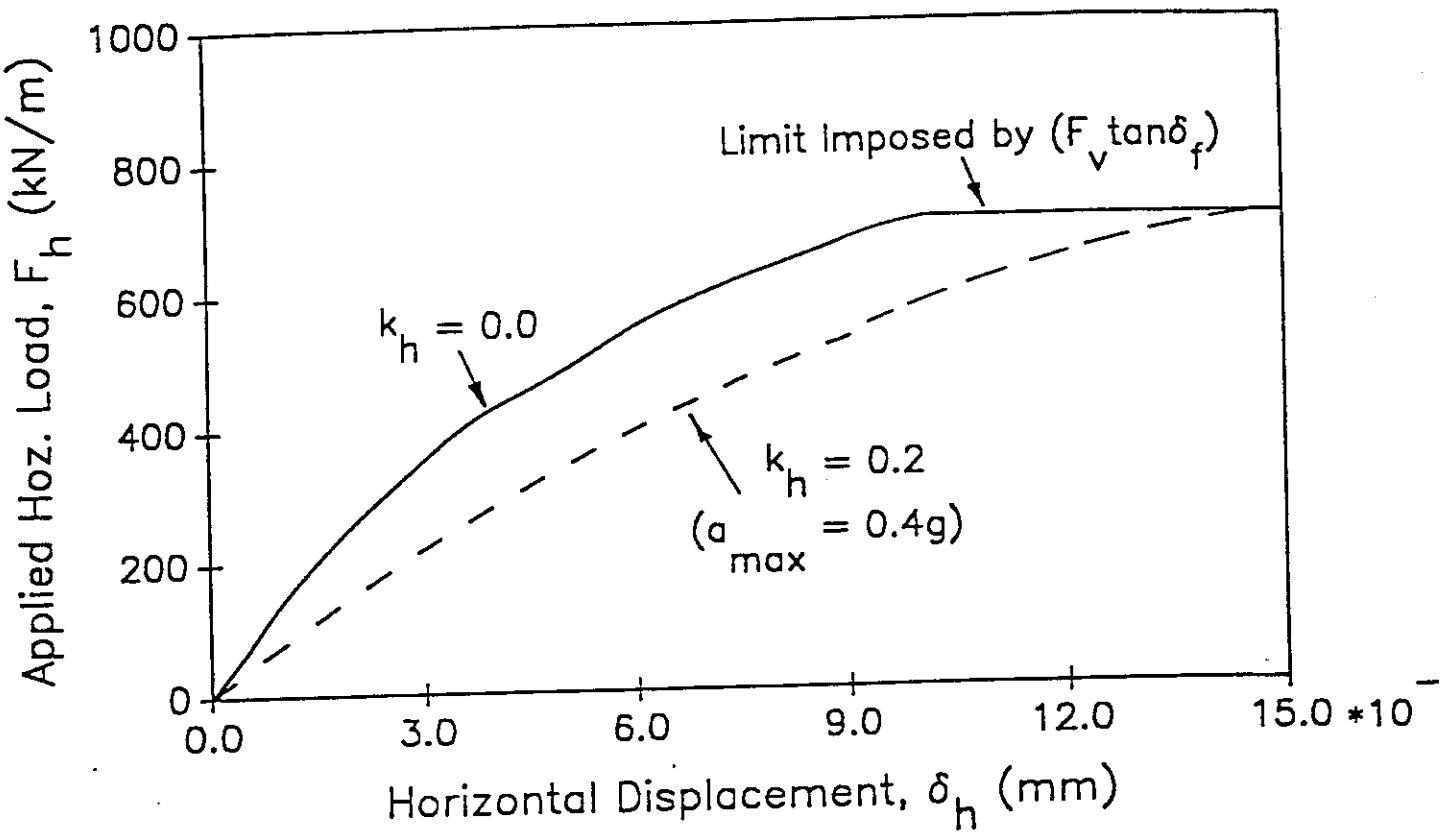

Fig. 19: F_h - δ_h Relationship at the Abutment face.

(a)

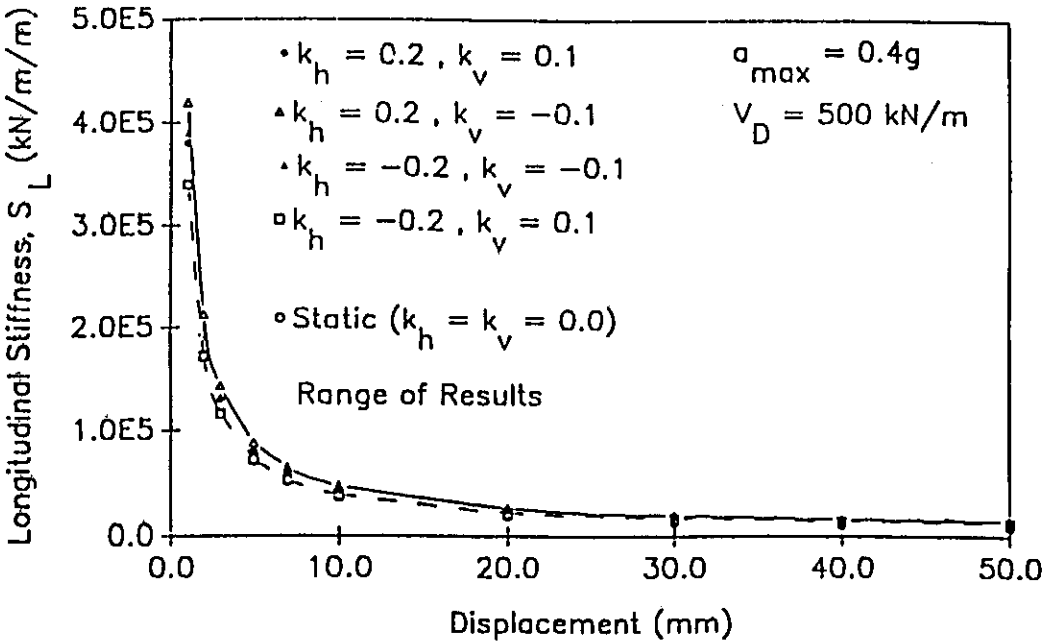
Longitudinal Stiffness, S_L (kN/m/m)
5.0E5
4.0E5
3.0E5
2.0E5
1.0E5
0.0
0.0
10.0
20.0
30.0
40.0
50.0
Displacement (mm)
• k_h = 0.2 , k_v = 0.1
▲ k_h = 0.2 , k_v = −0.1
▲ k_h = −0.2 , k_v = −0.1
▫ k_h = −0.2 , k_v = 0.1
∘ Static (k_h = k_v = 0.0)
Range of Results
a_{max} = 0.4g
V_D = 500 kN/m

(b)

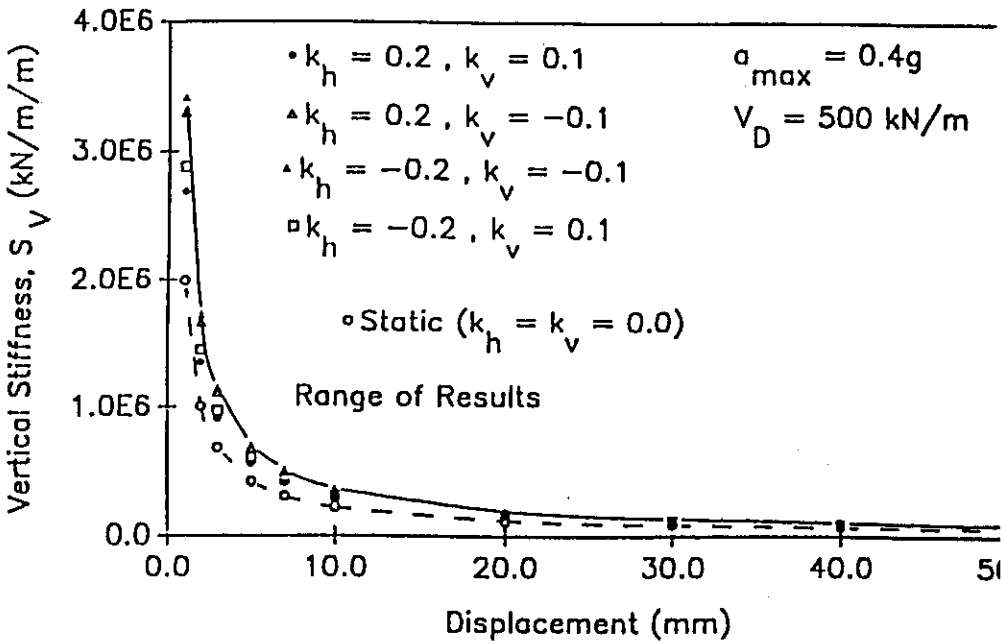
Vertical Stiffness, S_V (kN/m/m)
4.0E6
3.0E6
2.0E6
1.0E6
0.0
0.0
10.0
20.0
30.0
40.0
Displacement (mm)
• k_h = 0.2 , k_v = 0.1
▲ k_h = 0.2 , k_v = −0.1
▲ k_h = −0.2 , k_v = −0.1
▫ k_h = −0.2 , k_v = 0.1
∘ Static (k_h = k_v = 0.0)
Range of Results
a_{max} = 0.4g
V_D = 500 kN/m

(c)

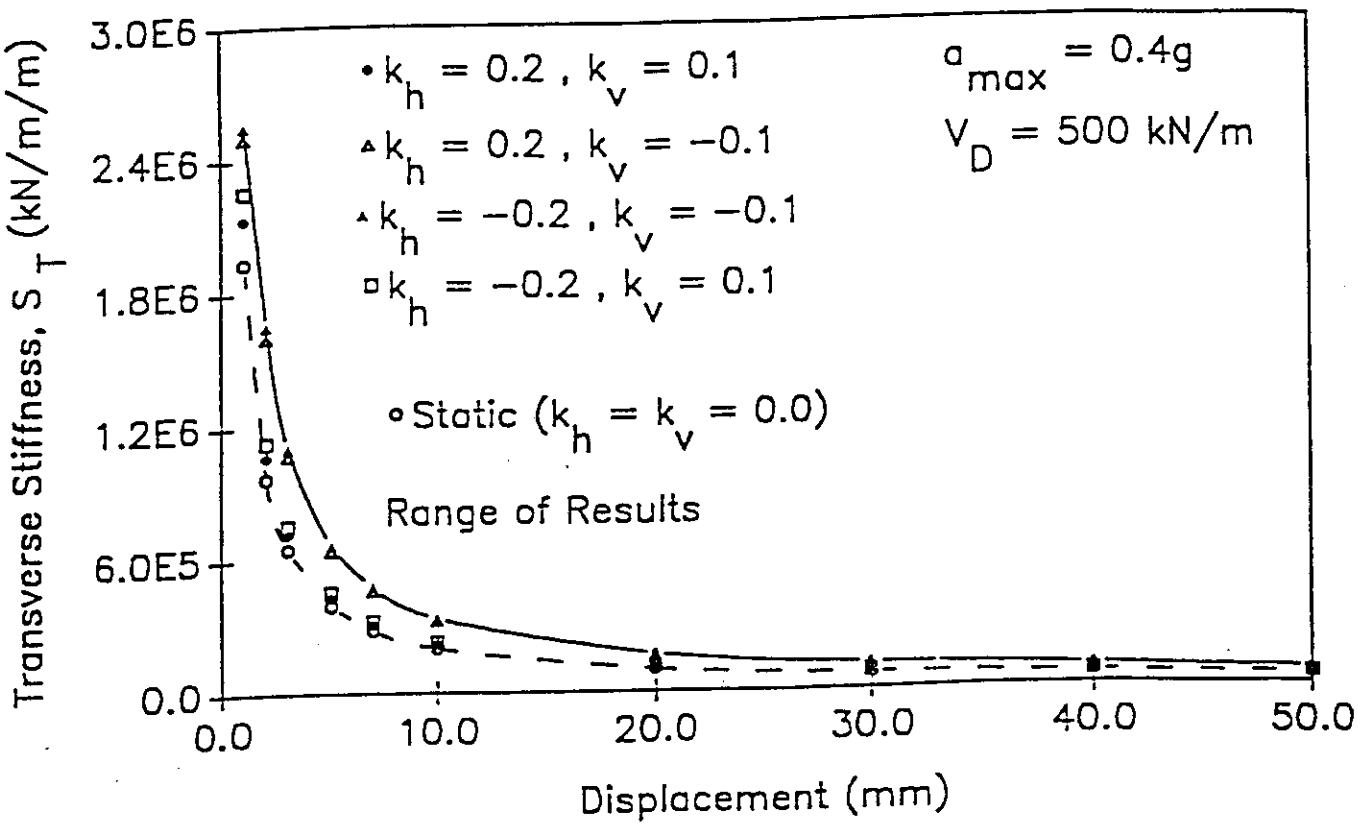

Fig. 20: Secant Translational Stiffnesses for all Cases (a) Longitudinal (b) Vertical and (c) Transverse.

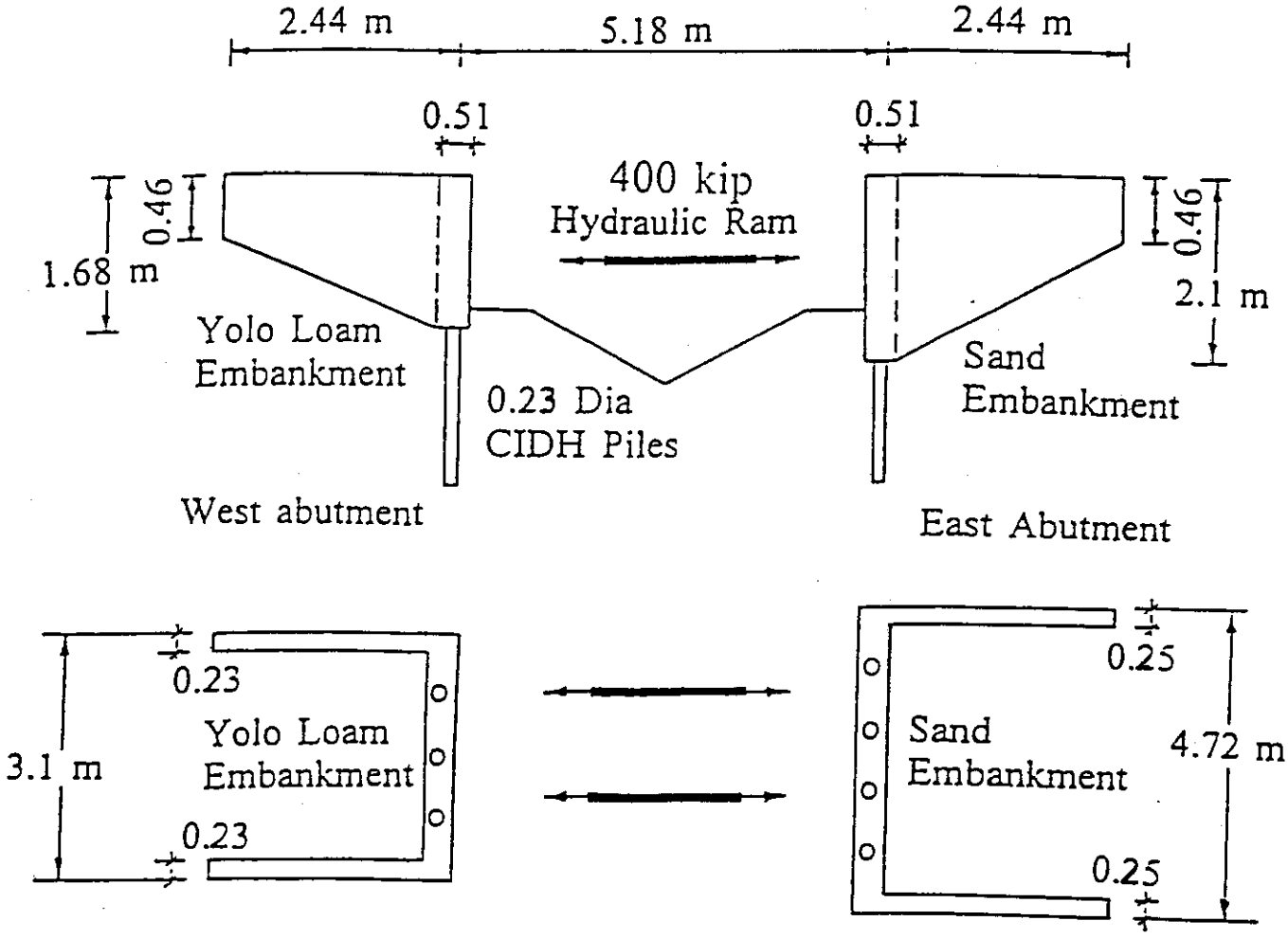

Fig. 21: Elevation and Plan Views of The Large-Scale Field Testing of Abutment (After Maroney et al., 1994).

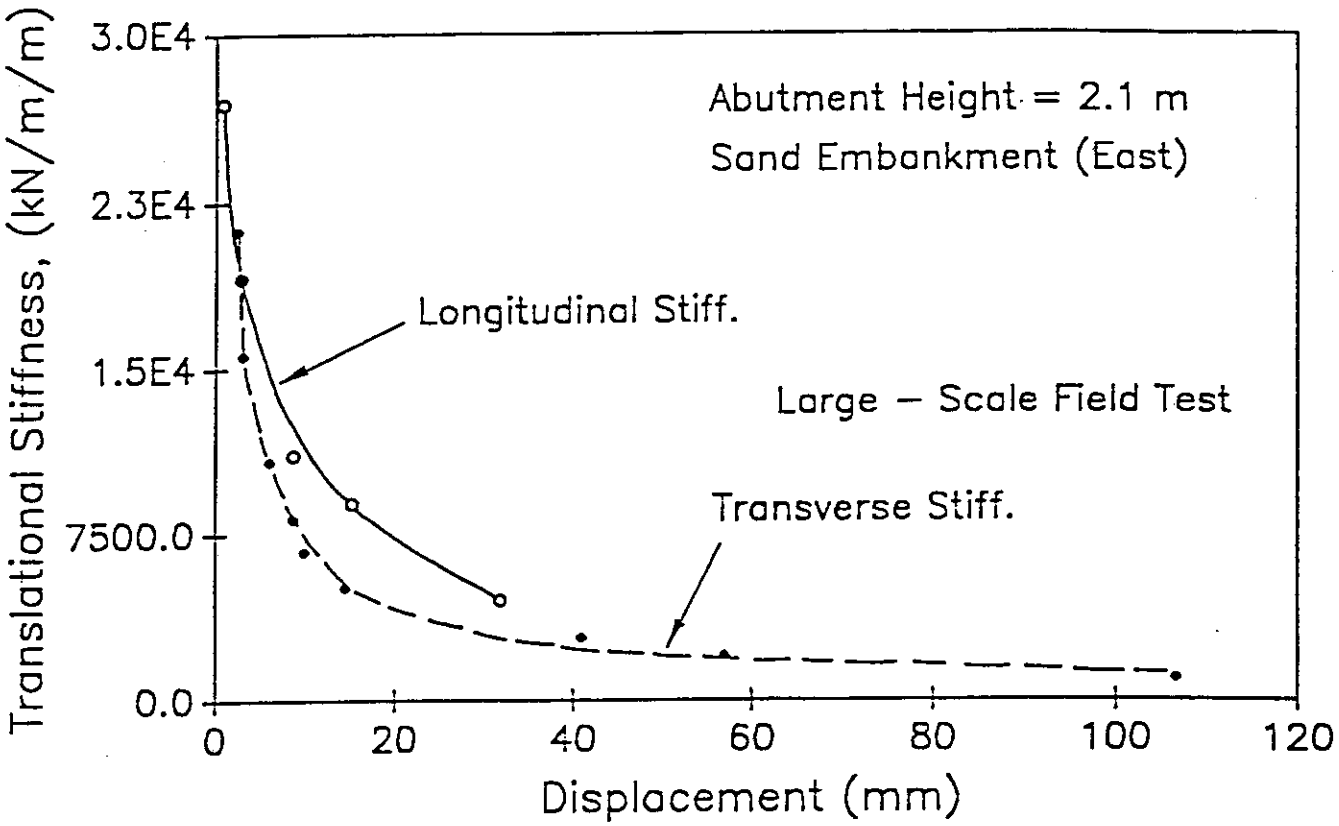

Fig. 22: Field Measured Secant Abutment Stiffnesses: Sand Embankment (After Maroney et al., 1994).

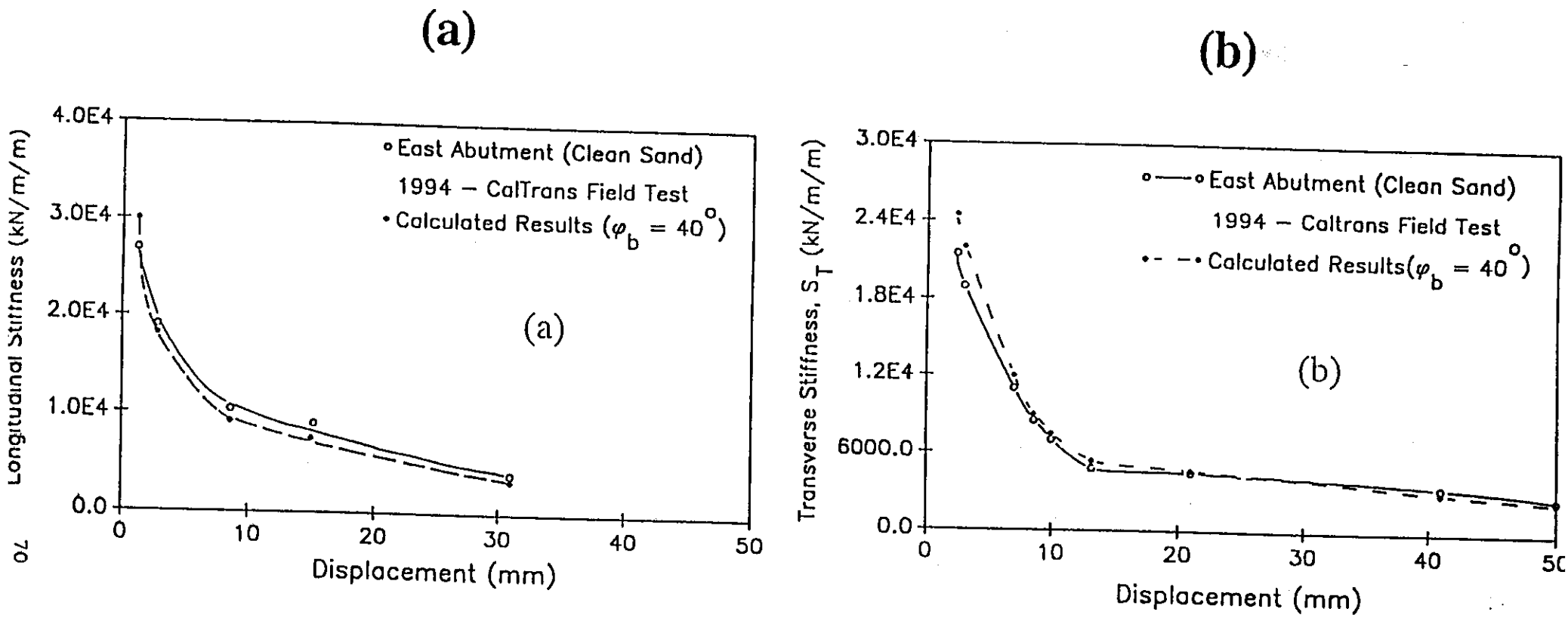

Fig. 23: Comparison Between Computed and Measured Abutment Stiffnesses (a) Longitudinal Stiffness (b) Transverse Stiffness.

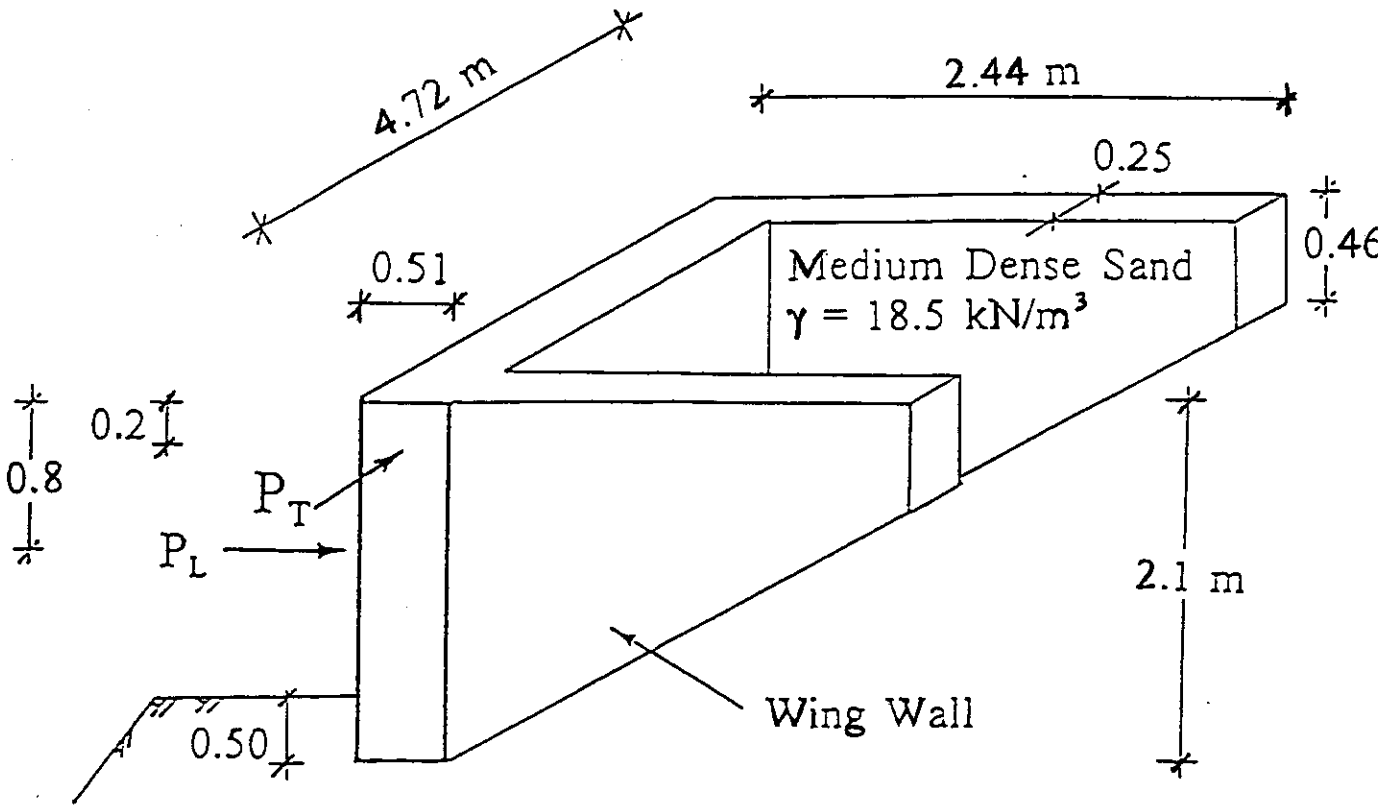

Fig. 24: Abutment Dimensions Used in Validation Study: Sand Embankment.

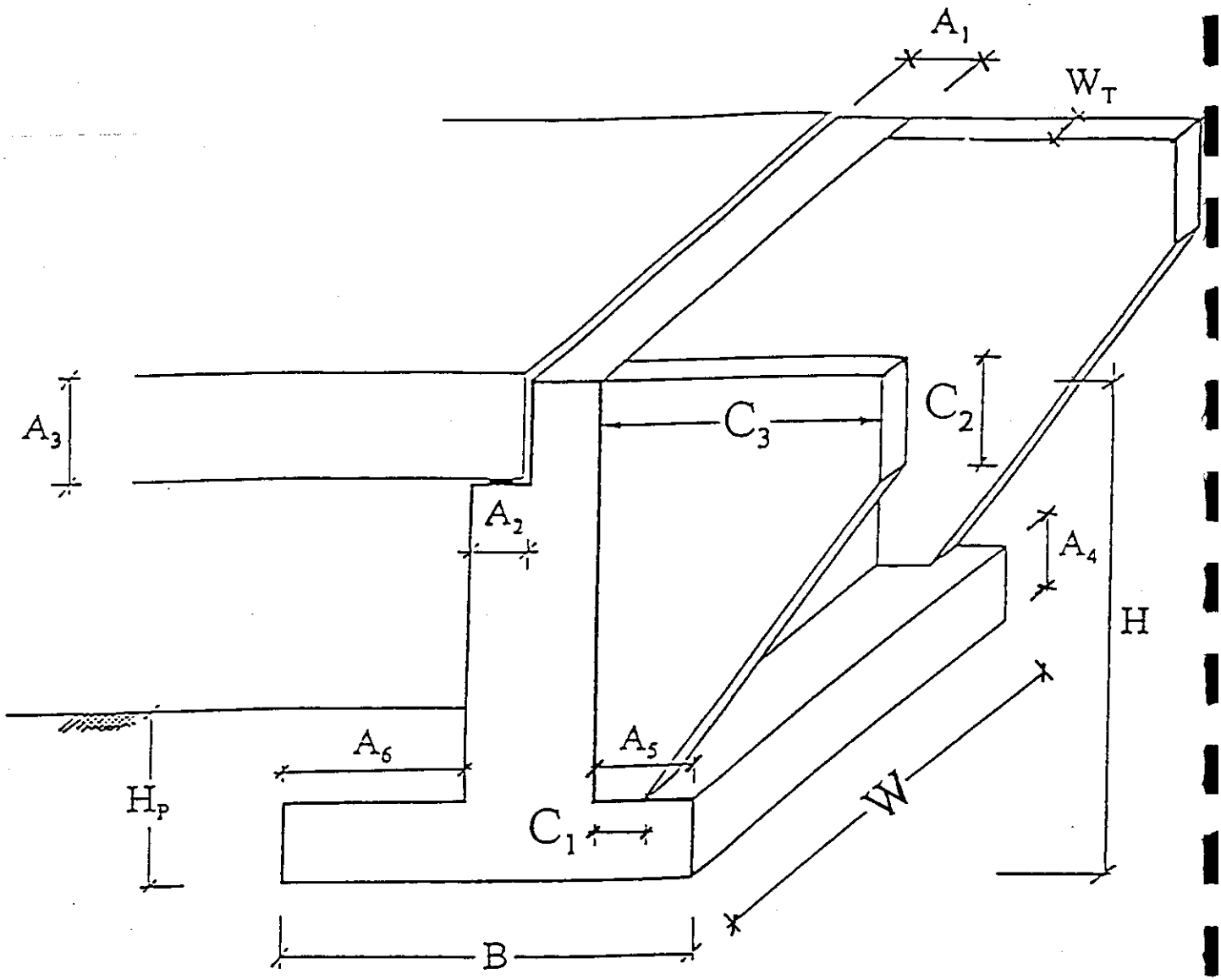

Fig. 25: Abutment Dimensions.

(a)

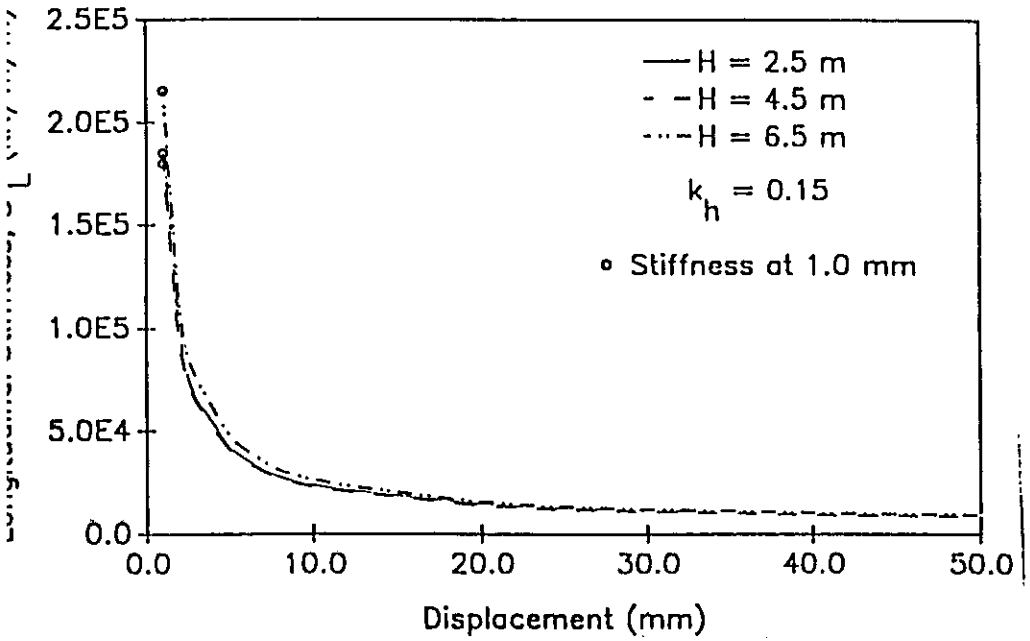
2.5E5
2.0E5
1.5E5
1.0E5
5.0E4
0.0
0.0
10.0
20.0
30.0
40.0
50.0
Displacement (mm)
H = 2.5 m
H = 4.5 m
H = 6.5 m
k_h = 0.15
Stiffness at 1.0 mm

(b)

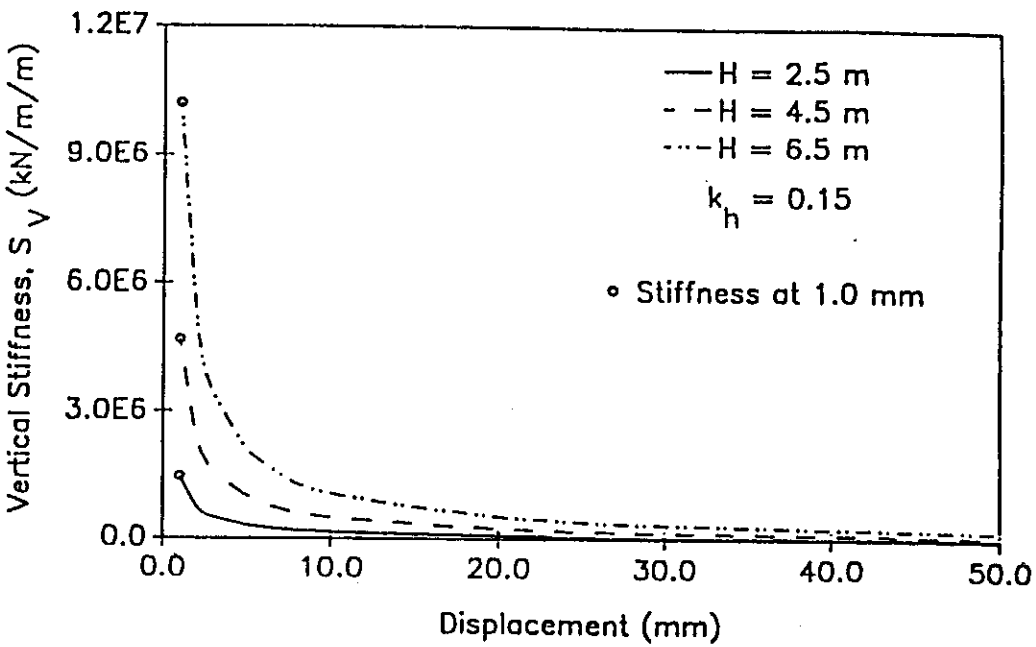
Vertical Stiffness, S_V (kN/m/m)
1.2E7
9.0E6
6.0E6
3.0E6
0.0
0.0
10.0
20.0
30.0
40.0
50.0
Displacement (mm)
H = 2.5 m
H = 4.5 m
H = 6.5 m
k_h = 0.15
Stiffness at 1.0 mm

(c)

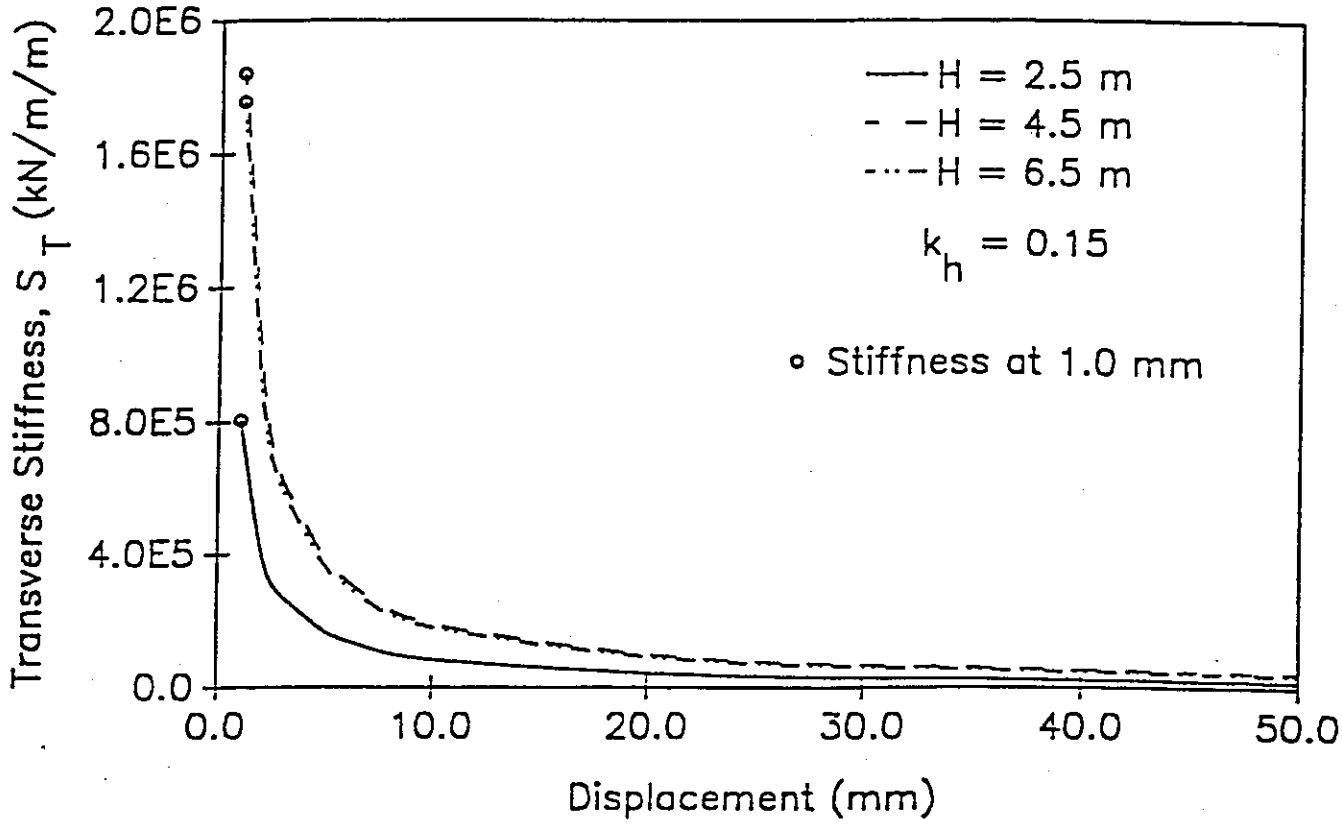

Fig. 26: Typical Variation of Translational Abutment Stiffnesses (a) Longitudinal (b) Vertical and (c) Transverse.

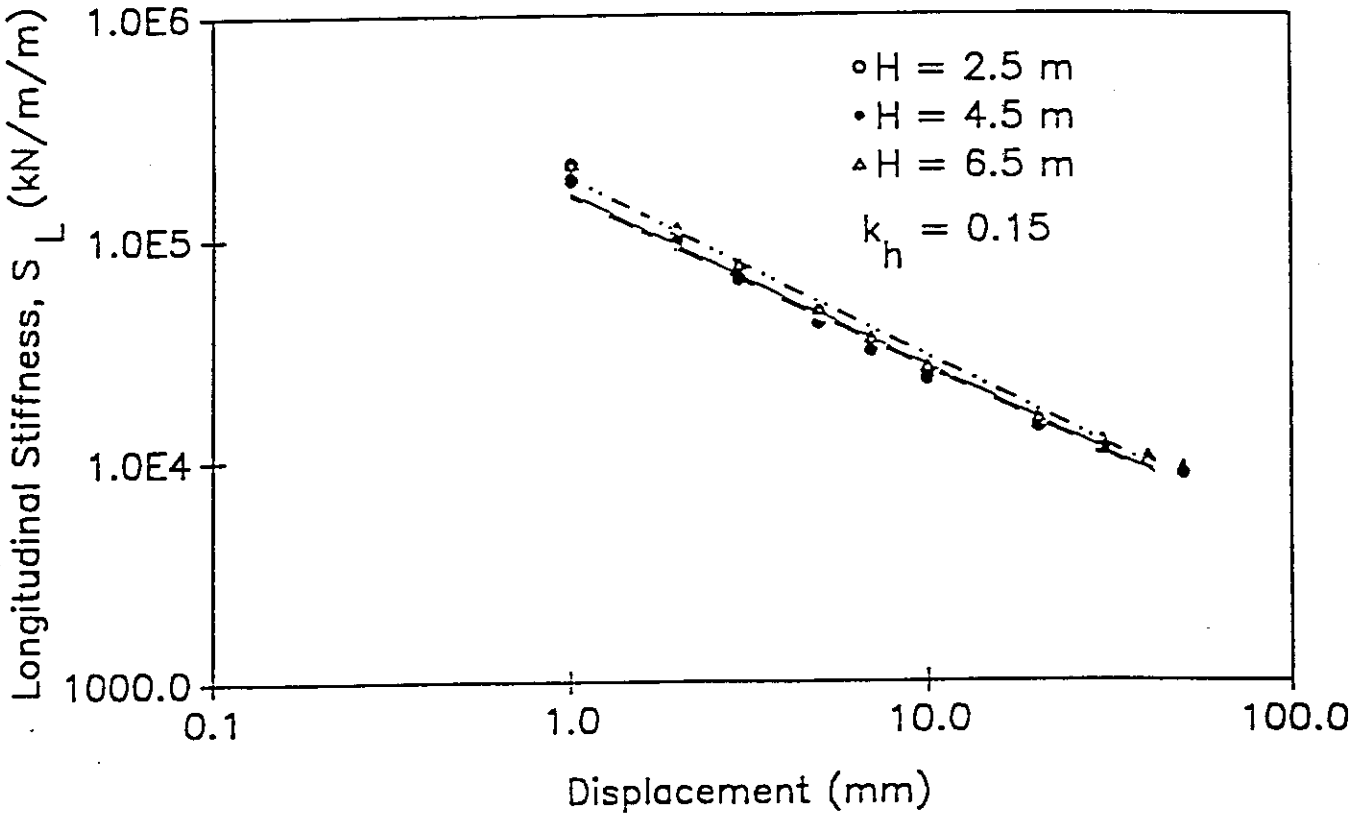

Fig. 27: Variation of Longitudinal Abutment Stiffness on a Log-Log Plot.

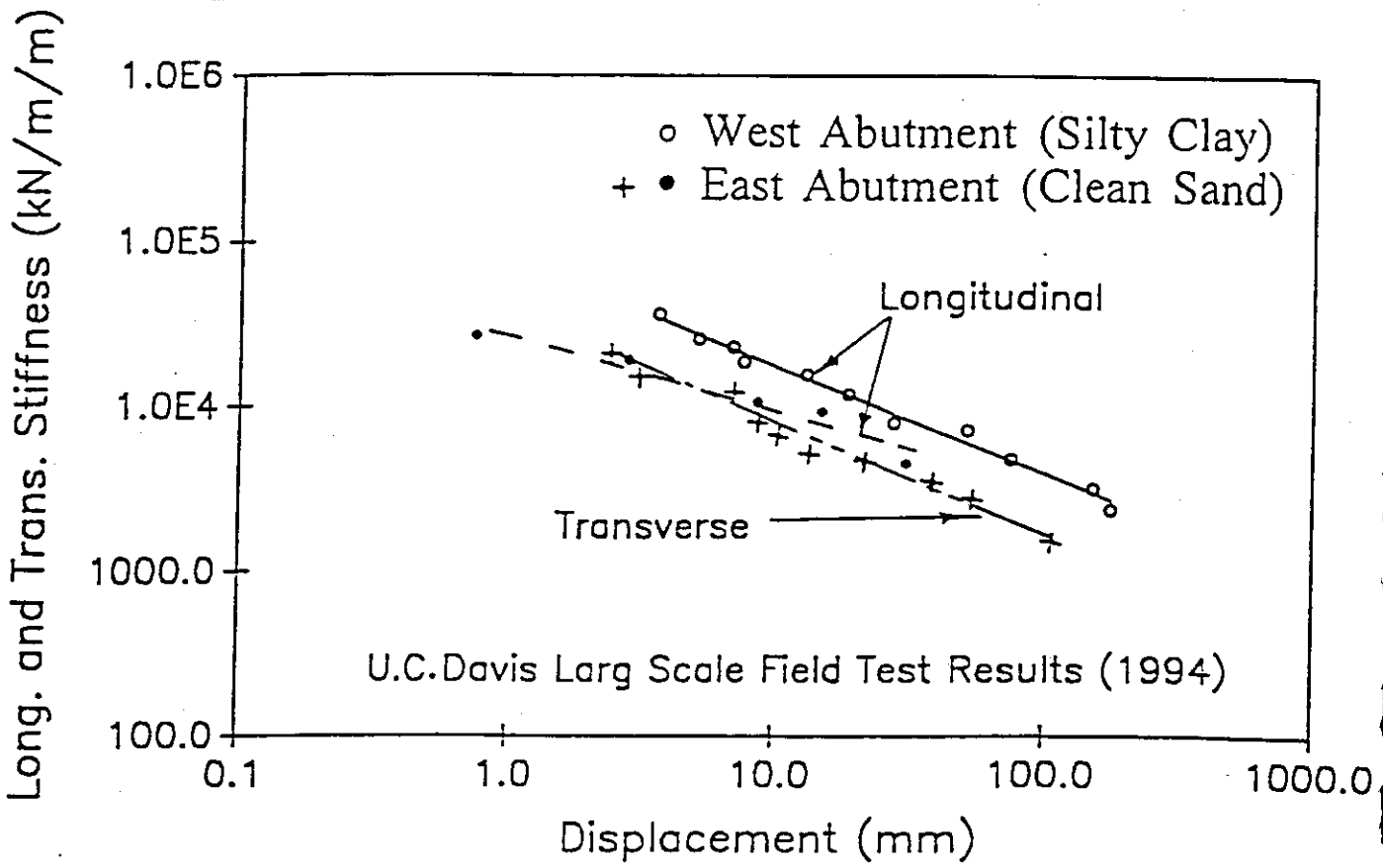

Fig. 28: Longitudinal and Transverse Abutment Stiffnesses from Field tests (After Maroney et al., 1994).

(a)

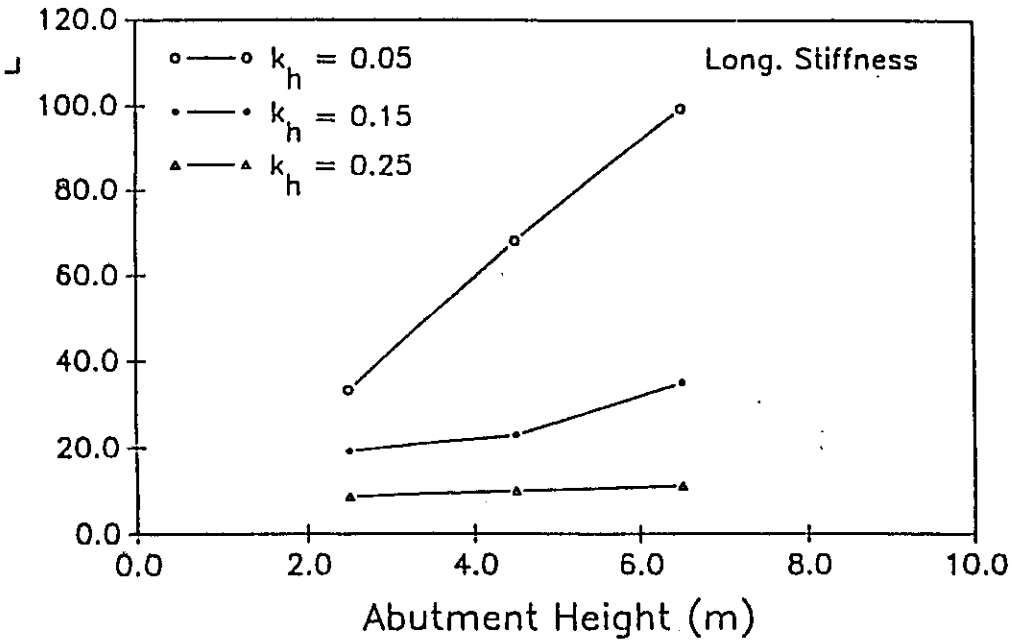
120.0
100.0
80.0
60.0
40.0
20.0
0.0
0.0
2.0
4.0
6.0
8.0
10.0
Abutment Height (m)
k_h = 0.05
k_h = 0.15
k_h = 0.25
Long. Stiffness

(b)

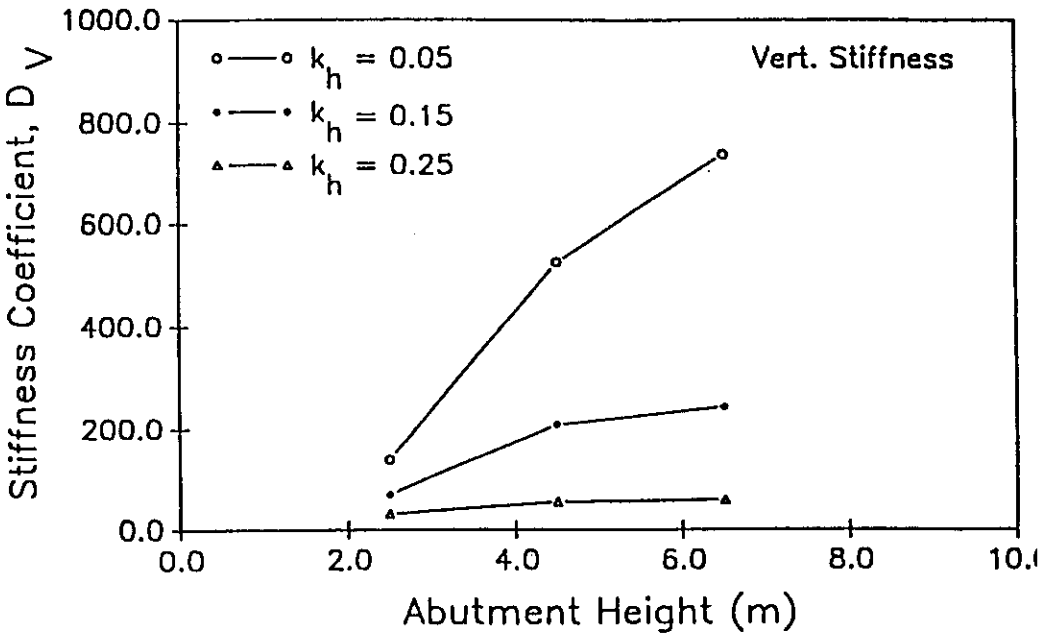
Stiffness Coefficient, D V
1000.0
800.0
600.0
400.0
200.0
0.0
0.0
2.0
4.0
6.0
8.0
Abutment Height (m)
k_h = 0.05
k_h = 0.15
k_h = 0.25
Vert. Stiffness

(c)

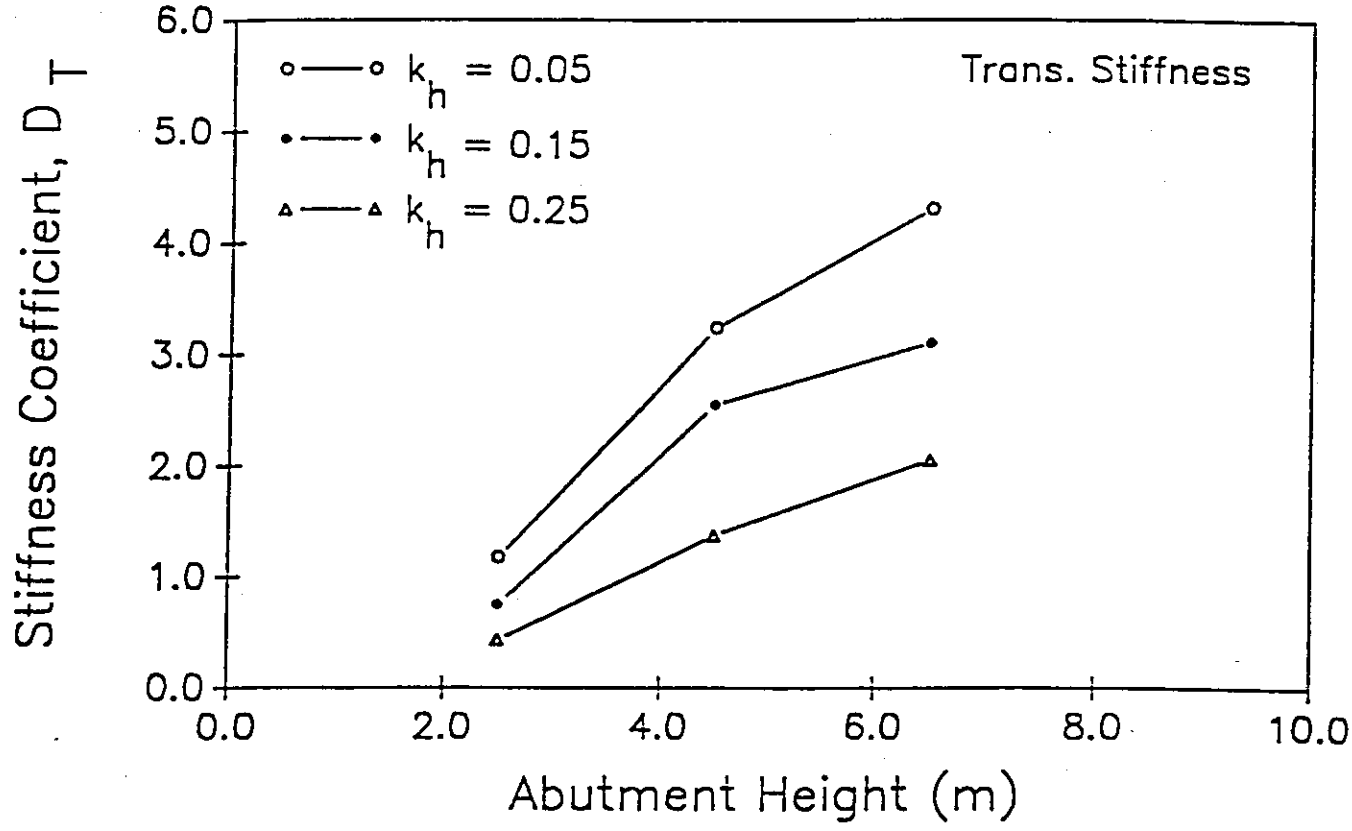

Fig. 29: Stiffness Coefficient, D_i (a) D_L - Longitudinal (b) D_V - Vertical and (c) D_T - Transverse.

(a)

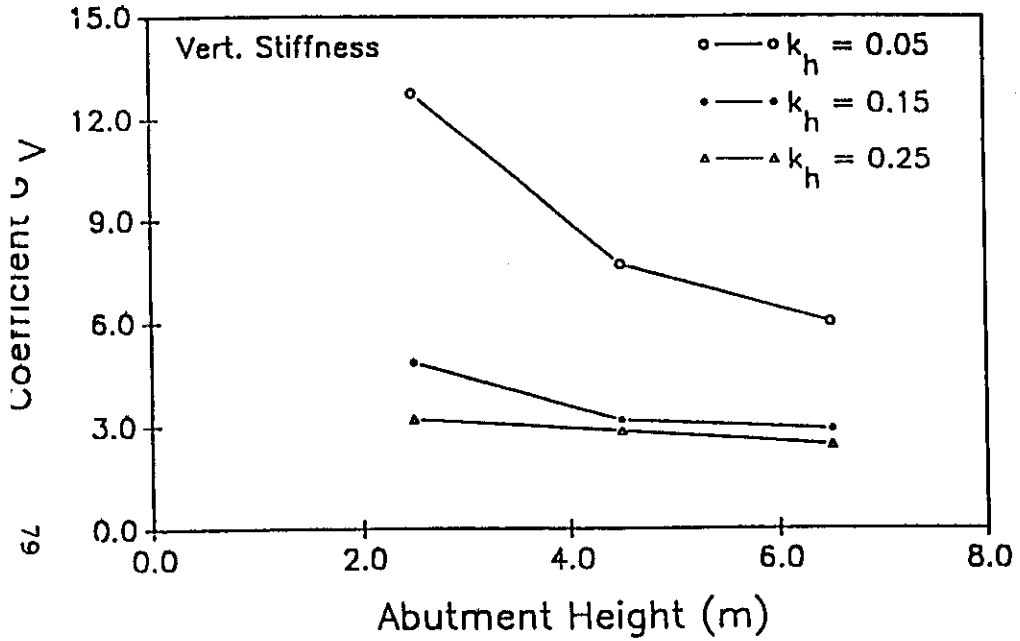
Vert. Stiffness
k_h = 0.05
k_h = 0.15
k_h = 0.25
Coefficient C_V
15.0
12.0
9.0
6.0
3.0
0.0
0.0
2.0
4.0
6.0
8.0
Abutment Height (m)

(b)

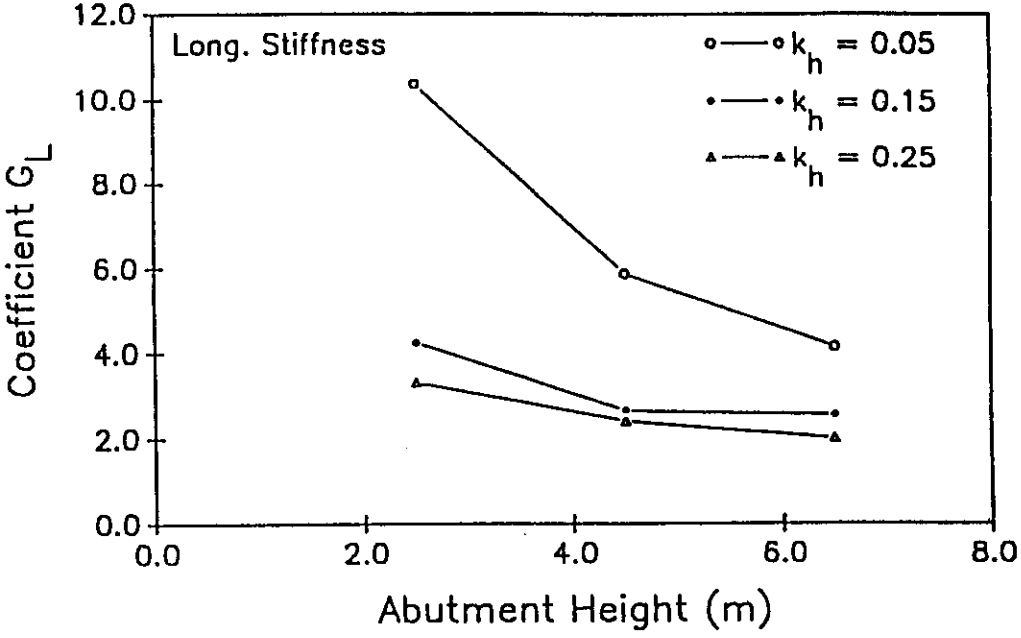
Long. Stiffness
k_h = 0.05
k_h = 0.15
k_h = 0.25
Coefficient C_L
12.0
10.0
8.0
6.0
4.0
2.0
0.0
0.0
2.0
4.0
6.0
8.0
Abutment Height (m)

(c)

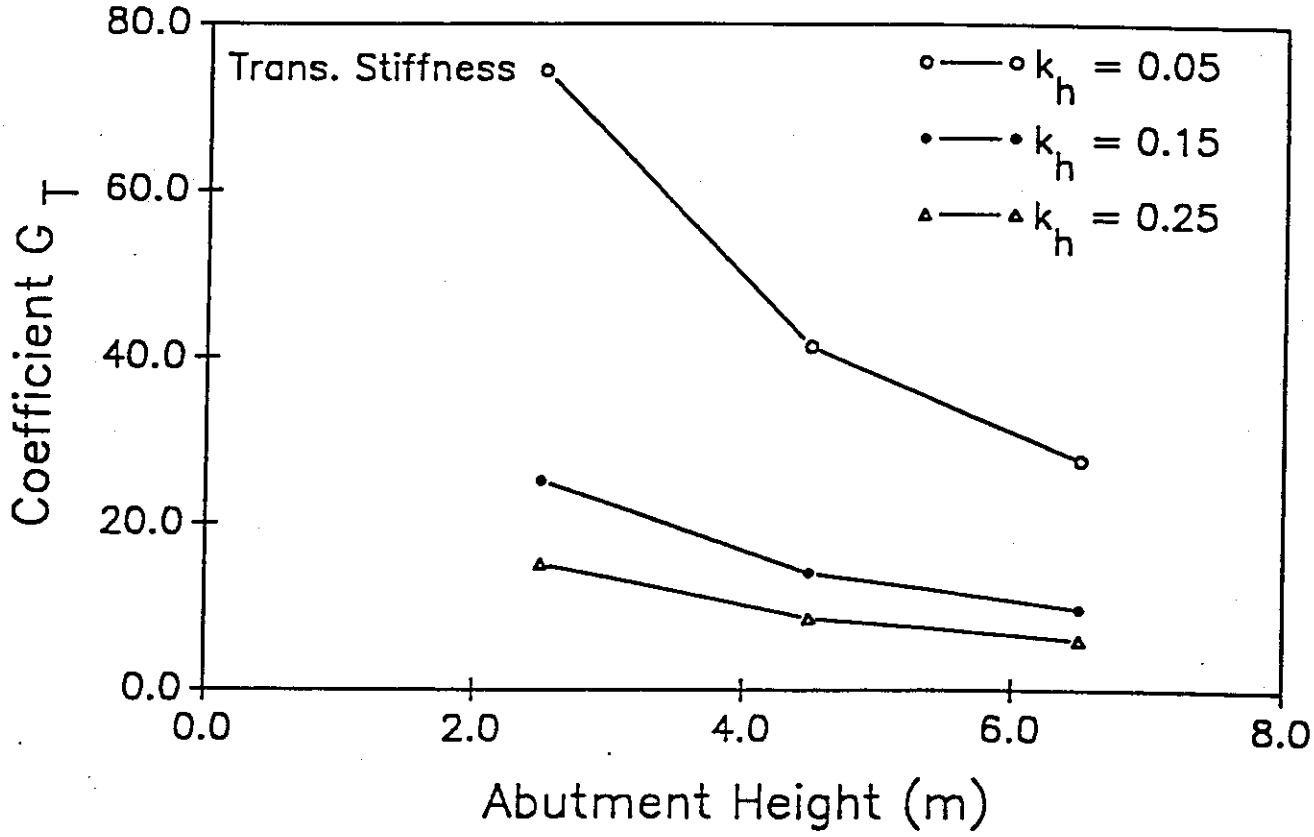

Fig. 30: Coefficient, G_i (a) G_L - Longitudinal (b) G_V - Vertical and (c) G_T - Transverse.

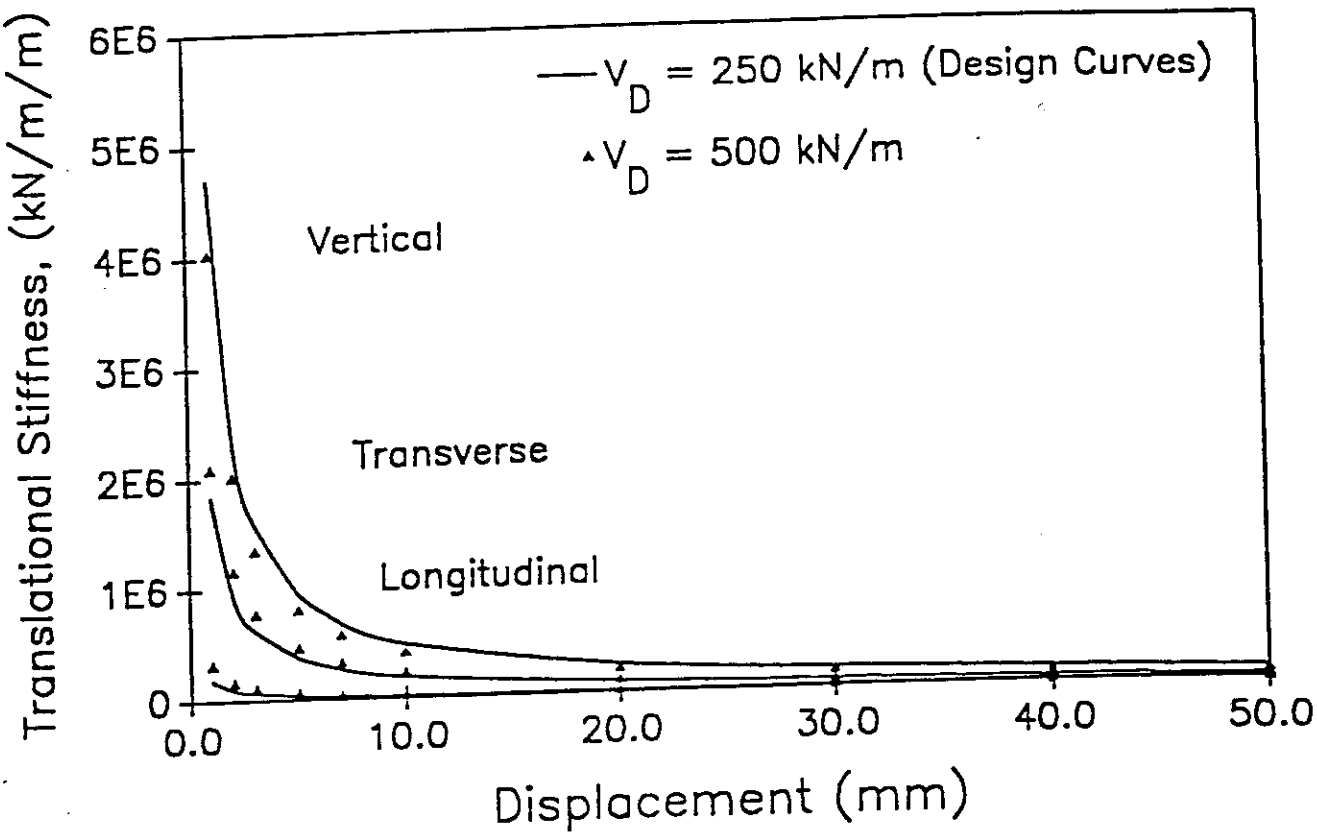

Fig. 31: Translational Stiffnesses from Design Curves and for the Case V_D = 500 kN/m.

(a)

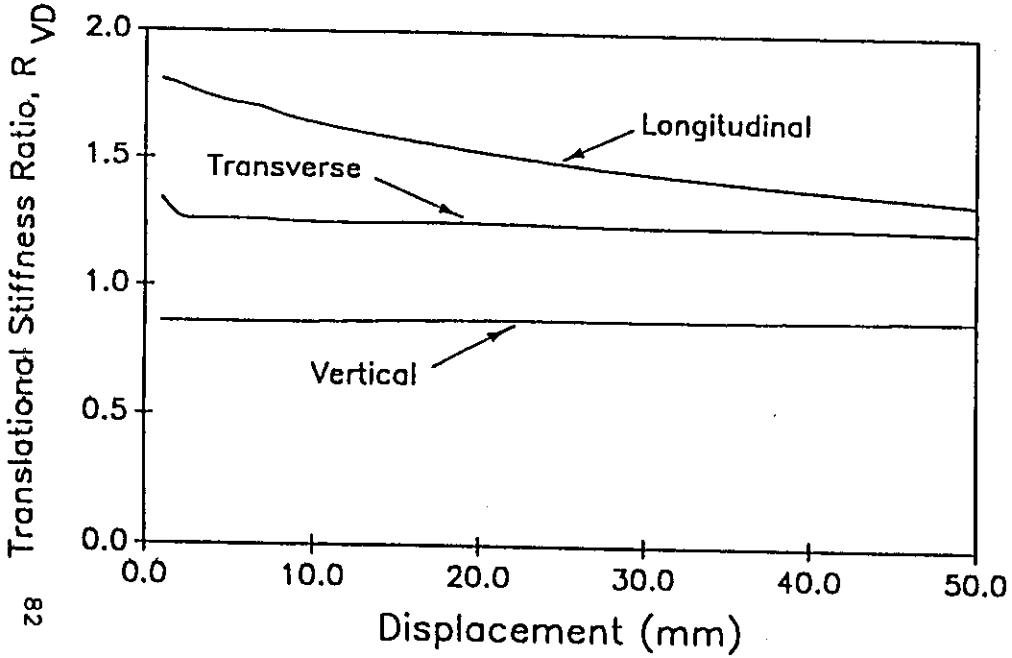
Translational Stiffness Ratio, R_{VD}
2.0
1.5
1.0
0.5
0.0
Longitudinal
Transverse
Vertical
0.0
10.0
20.0
30.0
40.0
50.0
Displacement (mm)

(b)

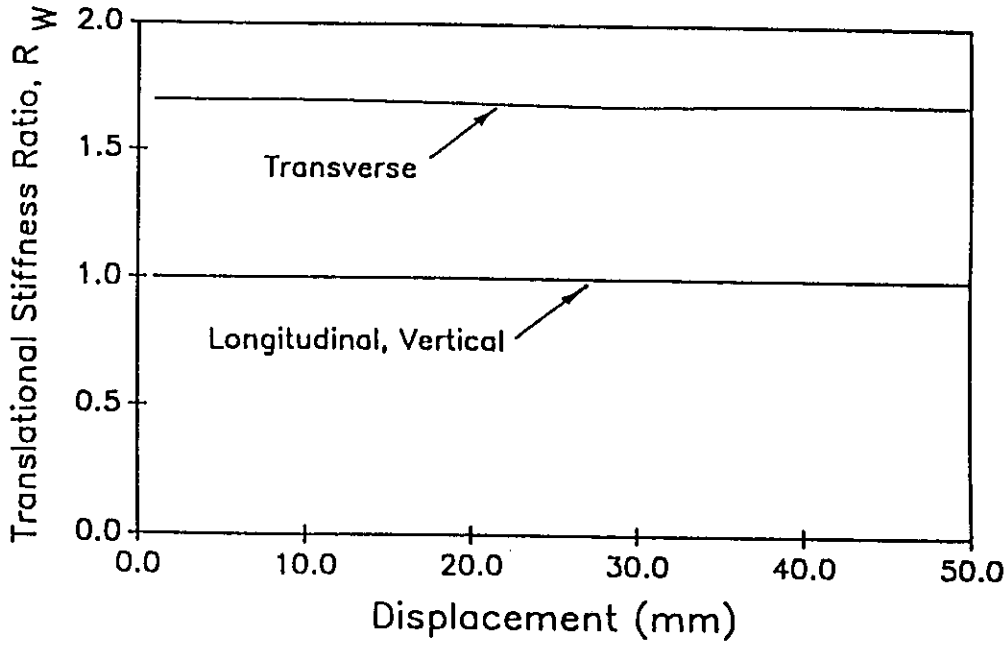
Translational Stiffness Ratio, R_W
2.0
1.5
1.0
0.5
0.0
Transverse
Longitudinal, Vertical
0.0
10.0
20.0
30.0
40.0
50.0
Displacement (mm)

(c)

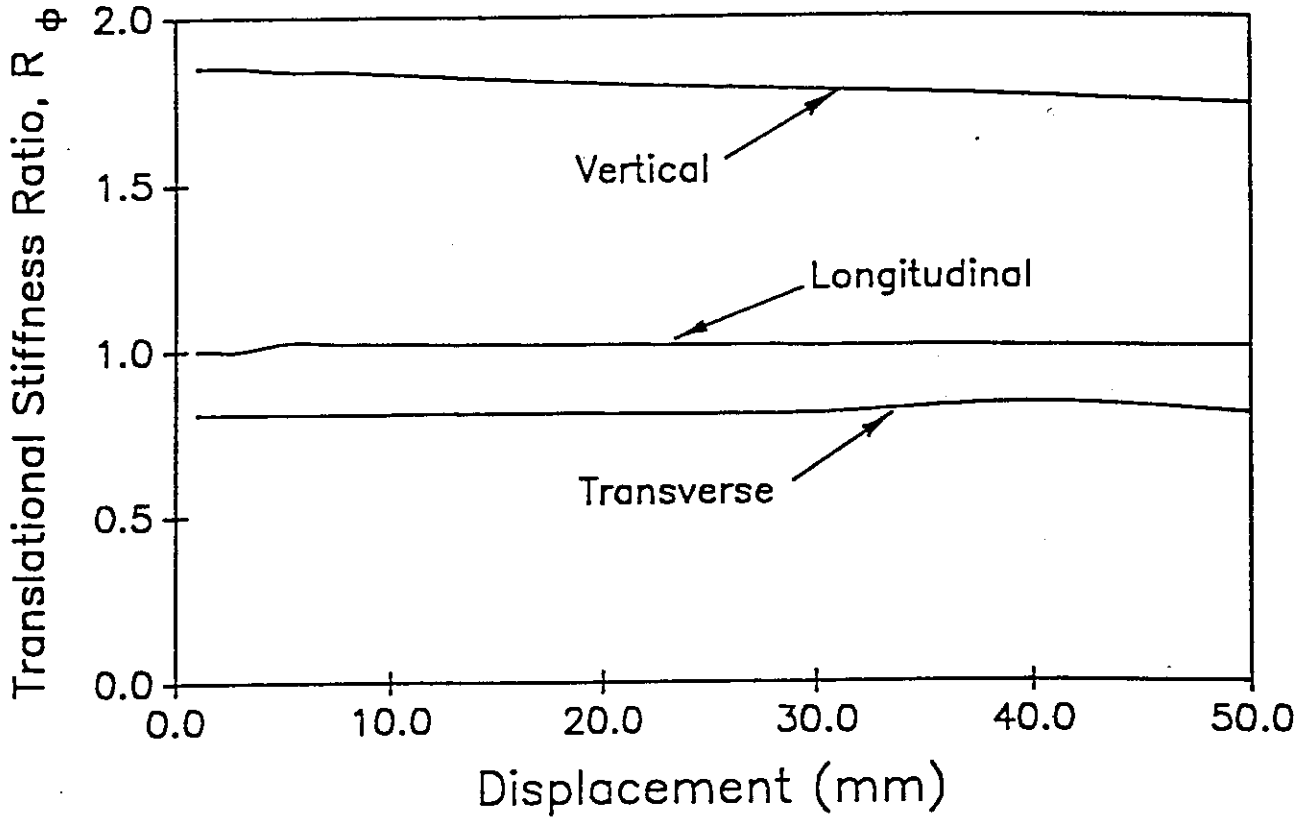

Fig. 32: Modification Factors (a) R_{VD} (b) R_W and (c) R_ϕ.

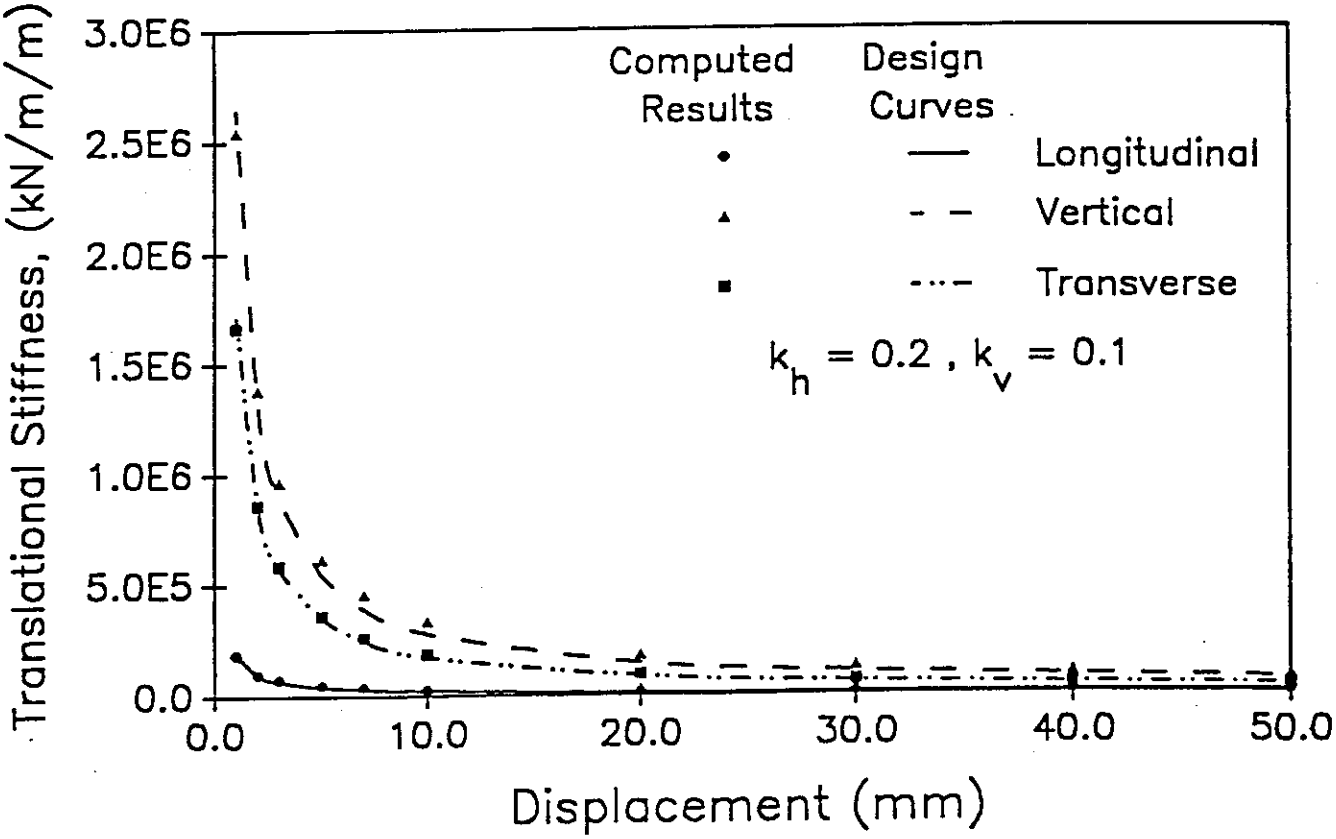

Fig. 33: Comparison of Translational Stiffnesses Given by Design Curves and the Proposed Approach.

Kenny C. Guinn, Governor

Nevada Department of Transportation
Tom Stephens, P.E. Director
Prepared by Research Division
Alan Hilton, Research Manager
(775) 888-7803
ahilton@dot.state.nv.us
1263 South Stewart Street
Carson City, Nevada 89712